DOCTORAL DISSERTATION SERIES

PUBLICATION: 5002

AUTHOR: Paul Raymond Barker, Ph. D., 1953
University of Michigan

TITLE: COSMIC RAY ELECTRONS AT ALTITUDES FROM SEA LEVEL TO 14,000 FEET

University Microfilms, Ann Arbor, Michigan, 1953

# COSMIC RAY ELECTRONS AT ALTITUDES FROM SEA LEVEL TO 14,000 FEET

by

Paul R. Barker

A dissertation submitted in partial fulfillment
of the requirements for the degree of
Doctor of Philosophy in the
University of Michigan
1952

Committee in charge:

Associate Professor W. E. Hazen, Chairman
Professor A. H. Copeland
Professor H. R. Crane
Professor D. M. Dennison
Assistant Professor R. W. Pidd

ABSTRACT

COSMIC RAY ELECTRONS AT ALTITUDES FROM
SEA LEVEL TO 14,000 FEET

Paul R. Barker

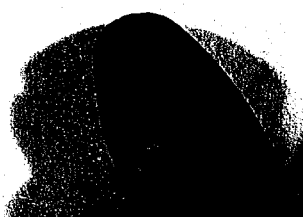
A cloud chamber containing aluminum and lead plates was used to measure the intensities of cosmic ray electrons at Ann Arbor, Echo Lake, and Mt. Evans. The chamber was triggered by a telescope of thin-walled aluminum counters. At each altitude measurements were made at zenith angles of $0^{\circ}$, $45^{\circ}$, and $60^{\circ}$.

Electrons are distinguished from other ionizing particles by their interactions with the metal plates. Electrons of low energy are absorbed in the aluminum plates at the top of the chamber, and their energies are estimated from the number of plates they penetrate. Electrons of high energy produce showers in the lead plates, and their energies are estimated from the size of the showers. Most penetrating particles (mesons and protons) pass through the plates without any observable interaction. Those which have sufficiently low energy to be absorbed in the plates can be distinguished from electrons by their high rate of ionization.

The observed intensities of penetrating particles are in good agreement with the results of other investigators, and therefore if there are any errors inherent in the method they must be of such a nature as to affect only the electrons and not the penetrating particles. Within the statistical uncertainties, the observed energy spectra of electrons are the same at the various altitudes and zenith angles, and an average spectrum, corrected for scattering in the counter telescope, is presented. The observed intensities

of electrons are given in terms of the intensities of penetrating particles. It is found that the decrease of intensity with zenith angle is much less than has been reported by other investigators. The value of the vertical intensity near sea level is in agreement with other results, but the increase of vertical intensity with altitude is somewhat slower than has previously been reported.

The expected number of electrons originating from μ-mesons is calculated as accurately as possible for the vertical direction at the altitude of Ann Arbor. An approximate method of calculation gives almost the same result and is used for other altitudes and zenith angles. An attempt is made to include the effects of scattering in the atmosphere on the intensities of these electrons. As was expected, the observed numbers of electrons are larger than the calculated numbers, and it is assumed the the excess electrons originate from neutral π-mesons produced by nuclear interactions in the atmosphere. This assumption is supported by the altitude dependence of the vertical intensity of the excess electrons, which is found to be exponential with an absorption length of $135 \pm 15$ gm $cm^{-2}$. The dependence of the excess electrons on zenith angle is much less steep than would be expected if the electrons preserved the directions of the primary particles from which they originated. This difference is greater than can be explained by the effects of scattering in the atmosphere. It is concluded, therefore, that the neutral π-mesons, from which the excess electrons supposedly originate, must have a relatively small average energy.



# PREFACE

The author wishes to express his heartfelt gratitude to Professor W. E. Hazen who suggested this problem and who provided friendly advice and guidance whenever it was needed or requested.

The research was supported in part by the joint program of the A.E.C. and the O.N.R., and was assisted by an A.E.C. Predoctoral Fellowship.

TABLE OF CONTENTS


| | | Page |
|---|---|---|
| LIST OF TABLES | | iv |
| LIST OF ILLUSTRATIONS | | iv |
| Chapter | | |
| I | INTRODUCTION | 1 |
| II | APPARATUS AND EXPERIMENTAL CONDITIONS | |
| | 2.1 The Cloud Chamber | 11 |
| | 2.2 Method of Triggering | 13 |
| III | INTERPRETATION OF DATA | |
| | 3.1 Analysis of the Photographs | 18 |
| | 3.2 Nature of the Penetrating Particles | 27 |
| | 3.3 Energy Calibration for Electrons of Low Energy | 28 |
| | 3.4 Energy Calibration for Electrons of High Energy | 37 |
| IV | EXPERIMENTAL RESULTS AND ERRORS | |
| | 4.1 Observed Numbers of Events | 42 |
| | 4.2 Errors due to Scattering | 45 |
| | 4.3 Other Experimental Errors | 50 |
| | 4.4 Correction for Finite Angle of Telescope | 54 |
| V | CALCULATION OF NUMBER OF ELECTRONS PRODUCED BY MESONS | |
| | 5.1 Previous Calculations | 57 |
| | 5.2 A More Accurate Method of Calculation | 58 |
| | 5.3 Approximate Calculations | 67 |
| | 5.4 Correction for Scattering in the Atmosphere | 69 |
| VI | DISCUSSION OF RESULTS AND CONCLUSIONS | |
| | 6.1 Counting Rates of Penetrating Particles | 72 |
| | 6.2 Energy Spectrum of Electrons | 76 |
| | 6.3 Intensities of Electrons | 80 |
| | 6.4 Electrons Originating from Nuclear Interactions | 88 |
| | 6.5 Summary of Results and Conclusions | 95 |
| | APPENDICES | |
| | I DEFINITIONS OF SYMBOLS | 98 |
| | II EFFECT OF SCATTERING ON ANGULAR DISTRIBUTION | 99 |
| | BIBLIOGRAPHY | 101 |

## LIST OF TABLES


| Table | | Page |
|---|---|---|
| I | Ionization of Slow Protons and Mesons | 24 |
| II | Energy Loss of Electrons in Duralumin and Brass | 32 |
| III | Energy Required to Penetrate Absorbers | 36 |
| IV | Energies of Showers in the Lead Plates | 40 |
| V | Numbers of Electrons Observed | 43 |
| VI | Other Experimental Data | 44 |
| VII | Correction Factors for Obtaining Directional Intensity from Counting Rates | 56 |
| VIII | Calculated Ratios of Electrons to Mesons | 69 |
| IX | Corrected Ratios of Electrons to Mesons | 70 |
| X | Counting Rates of Penetrating Particles | 72 |
| XI | Ratio of Number of Electrons Producing Showers of 4 or More Track Segments To Number Penetrating the Second Plate | 76 |
| XII | Integral Energy Spectrum of Electrons | 77 |
| XIII | Integral Energy Spectrum of Electrons Corrected for Scattering in the Central Counter | 77 |
| XIV | Observed Ratios of Electrons to Penetrating Particles | 82 |
| XV | Ratios of Electrons to Penetrating Particles from Greisen's data | 82 |
| XVI | Intensities of Excess Electrons with Energy >10 Mev | 90 |


## LIST OF ILLUSTRATIONS


| Figure | | Page |
|---|---|---|
| 1 | Nuclear Interaction Producing Two Photons | 5 |
| 2 | Arrangement of Counters | 15 |
| 3 | Typical Photographs | 21 |
| 4 | Typical Photographs | 22 |
| 5 | Range-Energy Graph for Duralumin and Brass | 34 |
| 6 | Number of Track Segments as a Function of Energy | 41 |
| 7 | Meson Spectrum Used for Calculation of Electrons | 64 |
| 8 | Zenith-Angle Dependence of Penetrating Particles | 75 |
| 9 | Integral Energy Spectrum of Electrons | 78 |
| 10 | Ratio of Electrons to Penetrating Particles as a Function of Zenith Angle | 84 |
| 11 | Intensities of Electrons from Nuclear Interactions | 91 |

# CHAPTER I

## INTRODUCTION

The cosmic rays observed near sea level consist primarily of μ-mesons, electrons, and photons. There is a very small proportion of protons, which increases rapidly as the altitude of observation is increased. Insignificant numbers of other types of ionizing particles are found in the lower part of the atmosphere. A few neutrons, and possibly other neutral particles, are present but are not usually observed in experiments using apparatus which is designed for the detection of charged particles.

The electrons and photons cannot be considered as independent of each other, although frequently only the electrons are observed. An electron, in passing through the air, generates photons when it is accelerated in the electric fields of nuclei (the process of bremsstrahlung). A photon of sufficient energy may interact with the electric field of a nucleus, producing an electron pair. Atomic electrons can be knocked out in collisions, both by electrons and by photons (Compton effect). Thus, a single energetic electron or photon will multiply into a shower containing many electrons and photons. The shower increases to a maximum number of electrons and photons, which depends on the initiating energy, and then it decreases again as more and more of the energy is absorbed by ionization. The theory of the development of showers has been worked out in considerable detail for the cases where certain simplifying assumptions can be made. This theory must be used in order to correlate the number of electrons

produced in the atmosphere with the number actually observed. Since the electrons and photons are so closely related, it is frequently convenient to refer to them collectively as the electronic component.

At one time it was believed that part of the electronic component was produced by primary electrons or photons incident at the top of the atmosphere and the rest by the decay and collision processes of mesons. However, in 1941 Schein, Jesse, and Wollan (41) made measurements at very high altitude and found no evidence of electronic radiation. They suggested the possibility that all of the electronic component is produced by mesons. More quantative experiments have been performed since that time, with similar results (20, 38). The recent experiment of Critchfield, Ney, and Oleska (9) indicates that electrons and photons of energies greater than 1 Bev constitute not more than a fraction of one percent of the primary particles. At ordinary latitudes (geomagnetic latitudes less than about 55°) the earth's magnetic field excludes electrons of less than 1 Bev. Perlow and Kissinger (30) have determined that less than 0.1% of the total energy flux of the primary radiation is due to photons of energies between 3.4 and 90 Mev. The results of all the experiments are consistent with the assumption that there are no primary electrons or photons.

Thus it is apparent that practically all of the observed electronic component must be produced in the atmosphere. However, the hypothesis that this production is due entirely to mesons was soon found to be untenable. In 1942 Rossi and Greisen (31) calculated the number of observable electrons originating from mesons and compared the results of the calculations with experimental values obtained by Greisen (14). The observed intensity of electrons was found to increase with altitude much more rapidly than the calculated intensity; so that, although they agreed fairly well at sea level, the calculated value was only half the observed value at an altitude of 4300 meters. The calculation involved many approximations and uncertainties, but these were not sufficient to explain the large discrepancy in the rate of variation with altitude. More precise calculations and comparisons (37) have confirmed this discrepancy, making it necessary to assume an additional source of electronic radiation in the upper atmosphere.

It is now known that the primary radiation is composed of protons, alpha particles, and heavier nuclei, which are rapidly absorbed and degraded in energy by nuclear interactions in the atmosphere. The simplest explanation for the large number of electrons at high altitudes is that they originate from these nuclear interactions. The most easily observed products of high energy nuclear interactions are $\pi$-mesons and nucleons, but there is considerable evidence

that electronic radiation is also produced (38). The most convincing of this evidence is probably that obtained by means of cloud chambers containing lead plates. Several investigators (8, 11, 13) using apparatus of this sort have obtained pictures of nuclear interactions producing both electron showers and heavier particles. A good example of such a photograph was obtained by chance during the preliminary stages of the present investigation and is shown in Figure 1. The generally accepted hypothesis concerning the mechanism by which electronic radiation originates from nuclear interactions is that neutral $\pi$-mesons, which decay with an extremely short lifetime into two photons, are produced. The event of Fig. 1 is in excellent agreement with this hypothesis (1). Evidence for the existence of neutral $\pi$-mesons has been obtained from nuclear interactions produced by protons from a cyclotron (4) and by photons from a synchrotron (45).

The greatest uncertainty in the early calculations of the number of electrons produced by mesons came from the fact that the decay scheme of the $\mu$-meson was unknown. It was known that an electron is produced, but the amount of energy given to the electron was undetermined. This uncertainty affected the magnitude of the electron intensity but had little effect on the variation with altitude. It was frequently assumed that in addition to the electron a single neutrino is emitted. (At least two particles are required

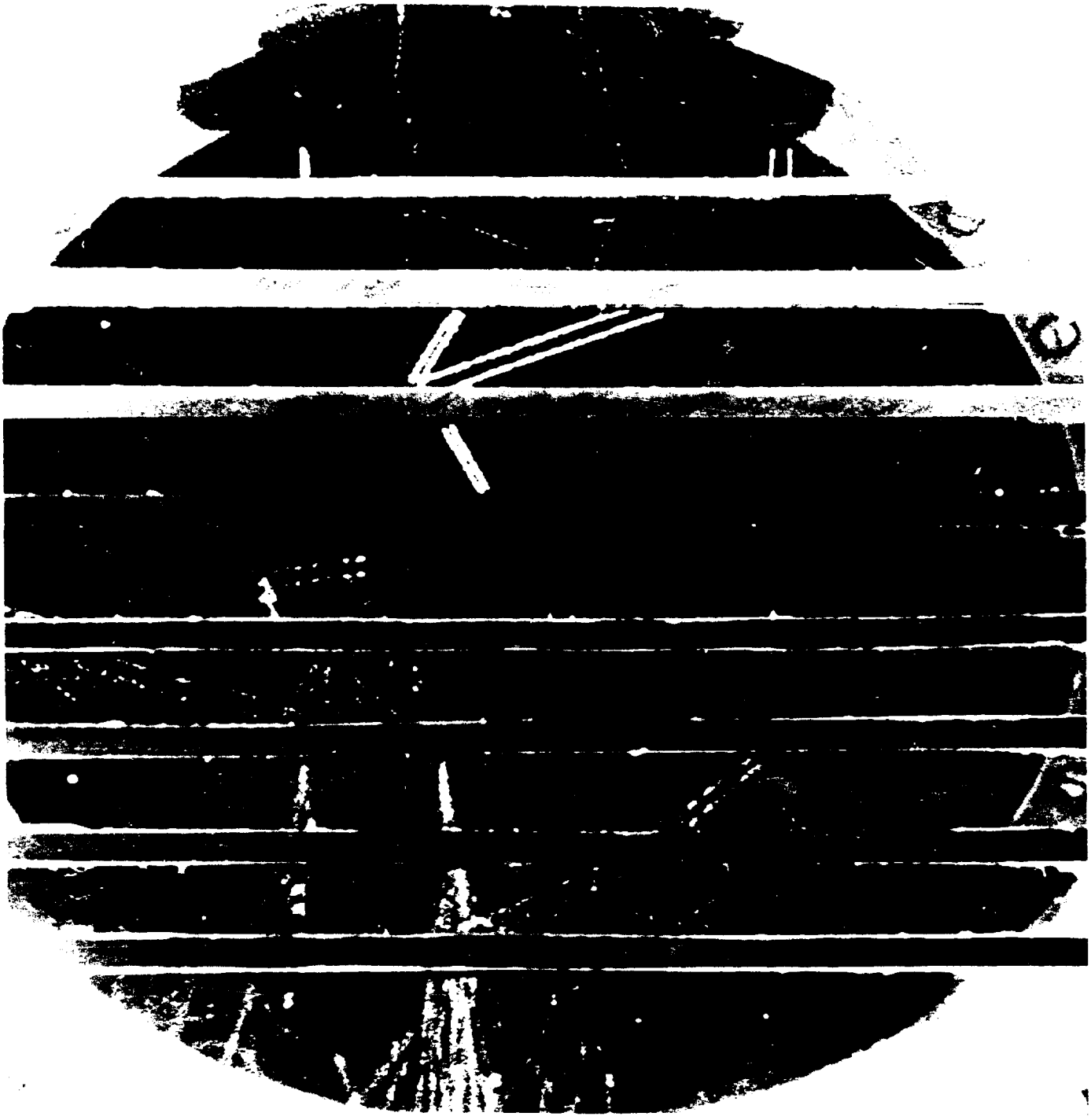


Fig. 1 Nuclear interaction producing two photons.

in order to conserve energy and momentum.) According to this assumption the electron receives one half the energy of the meson. However, the experimental evidence seemed to indicate that the number of electrons observed near sea level is smaller than would be expected in that case (15, 37). Consequently, for a number of years one of the main points of interest in studying the electron intensity was the attempt to determine how much of the energy of the decaying mesons appears in the electronic component and thus to gain a better understanding of the decay process of the meson.

At present the situation is somewhat different, since the energy spectrum of the decay electrons has been determined by observations of mesons decaying at rest (24, 39), and it is now well established that the μ-meson decays into one electron and two neutral particles which are probably neutrinos, with the electron receiving on the average approximately one third of the energy. Therefore, it no longer appears profitable to try to obtain new information about the decay of μ-mesons by the indirect method of studying the intensities of cosmic rays. It seems more reasonable to assume that the decay process is known and that the number of electrons originating from mesons can be calculated with an accuracy limited only by the shower theory and the available data on the intensities of mesons at various altitudes. Then, by subtracting the calculated intensity of electrons

from the observed intensity, it is possible to find the intensity of electrons from nuclear interactions. It is known (37) that the number of nuclear interactions in the atmosphere varies approximately as $e^{-h/125}$, where h is the depth from the top of the atmosphere in gm $cm^{-2}$. Consequently, electrons from this source might be expected to have a very strong dependence on both altitude and zenith angle. Electrons observed at large zenith angles near sea level should consist predominantly of those produced by secondary processes of mesons, and electrons observed near the vertical direction at high altitude should consist largely of those originating from nuclear interactions.

The measurements of Greisen (14), made in 1942 at several altitudes and zenith angles, provide the best data yet published from which the directional intensities of the electrons can be derived. He used a counter telescope, consisting of six G-M counters operated in coincidence, and measured the counting rate with and without lead absorber between the counters. The lead was of sufficient thickness (167 gm $cm^{-2}$) to eliminate all but a negligible fraction of the electrons. The hard component, defined as those particles which can penetrate the lead, is composed mainly of mesons; while the soft component, measured by the difference in the two counting rates, consists mostly of electrons.

The major source of uncertainty in Greisen's results is the loss of particles caused by scattering in the brass walls of the counters. This effect is especially serious for electrons of low energy, which may scatter through considerable angles while traversing a relatively small amount of material. There is also some uncertainty as to the number of slow mesons and protons in the soft component.

The Wilson cloud chamber offers several advantages over G-M counters for the measurement of electron intensities. It is possible to distinguish with a high degree of reliability between energetic electrons and heavier particles by placing several lead plates within the chamber. Electrons will undergo radiative multiplication in the lead, forming small showers which are easily observed. For particles of equal velocity the probability of radiation is inversely proportional to the square of the mass. Therefore, since the mass of a meson is over 200 times that of an electron, the probability that mesons or heavier particles will initiate showers in the lead is insignificant. In order to facilitate the recognition of low energy electrons, a few aluminum plates can be placed above the lead plates. Electrons of low energy will be absorbed in the aluminum, losing their energy primarily by ionization. Mesons or heavier particles which have sufficiently low energies to be stopped in any one of the plates will exhibit considerably greater than minimum ionization in the gas above the plate without

showing the large amount of scattering in the gas which is characteristic of an electron of the same ionization.

Very little information is available at present on the energy distribution of electrons in cosmic rays. Greisen (15), using absorption methods with G-M counters, has made measurements at low altitude and integrated over all directions. Hazen (17), by means of a cloud chamber with lead plates, has determined the spectrum of high energy electrons and photons at 10,000 feet.

By using a cloud chamber containing aluminum and lead plates, it is possible not only to detect electrons with considerable accuracy but also to obtain information about their energy spectrum. The energies of the slow electrons can be determined from their ranges, that is, from the number of aluminum plates they traverse. The energies of the fast electrons can be estimated from the development of the showers they produce. It would be possible to measure energies with greater accuracy by the use of a magnetic field, but that method would be much more laborious and expensive and would involve apparatus which is not easily transported to high altitude.

Other advantages of the cloud chamber method are that the effect of scattering can be reduced and that corrections for side showers are unnecessary. In order to count only particles coming from a given direction, the chamber must be

triggered by a telescope of G-M counters placed above it and defining a small solid angle. If thin-walled aluminum counters are used, they will introduce a very small amount of scattering. A few particles will be lost by scattering in the top wall of the chamber, but all those which reach the invisible region can be counted, regardless of how they scatter in the absorbing plates. Particles are counted only when their tracks are seen emerging from the top wall of the chamber in a region directly below the counters. Air showers involving many particles are easily recognized and need not be counted. The greatest disadvantage of this method is that the counting rates are low and it takes a long time to accumulate the data.

To supply the obvious need for more information on the directional intensities and energies of electrons, the present investigation was undertaken, using a cloud chamber in the manner described above. Measurements were made at Ann Arbor, Echo Lake and Mt. Evans, at zenith angles of 0°, 45°, and 60°. Calculations were made of the intensities of electrons resulting from mesons, and the differences between those values and the observed values are considered to represent the intensities of electrons originating from nuclear interactions.

## CHAPTER II

## APPARATUS AND EXPERIMENTAL CONDITIONS

### 2.1 The Cloud Chamber

The main body of the cloud chamber used during this investigation was a Pyrex cylinder of inside diameter 29 cm and length 45 cm. The average wall thickness in the region below the counters was 0.63 cm. The maximum internal pressure was controlled by compressed air behind a rubber diaphragm, and the expansion was accomplished by releasing the compressed air to the atmosphere. The chamber contained air saturated with a mixture of three parts ethyl alcohol and one part distilled water. The minimum pressure was maintained at about 17 cm of Hg above atmospheric pressure and the expansion ratio was adjusted to give the best tracks by varying the maximum pressure.

The chamber was photographed from the front end by a stereoscopic camera. The two lenses of the camera viewed the tracks with an included angle of $4^{\circ}$. Illumination was provided by two G. E. FT-422 flash tubes mounted in parabolic reflectors, which were directed at angles of $135^{\circ}$ to the line of sight of the camera. Each flash tube was connected to a capacitance of 300 mf charged to 1500 volts, and was fired by means of a spark coil.

Eight absorbing plates were used in the chamber. The top plate was 0.32 cm of aluminum, the next two were each 0.64 cm of aluminum, the fourth was 0.66 cm of brass, and the bottom

four were each 0.64 cm of lead. The aluminum used was an alloy, 24S, containing 4.5% Cu, 1.5% Mg, and 0.6% Mn, with a density of 2.77 gm $cm^{-2}$. The plates were tilted so that only their edges were visible to the camera. A 0.008 cm phosphor bronze foil was fastened to the upper surface of the top plate and four short vertical wires were soldered to the foil. These wires formed a rectangle outlining the region which could be traversed by particles which passed, without scattering, through the counters and the upper wall of the chamber. The rectangle measured approximately 4.0 by 10.5 cm, with the short dimension parallel to the axis of the chamber. The depth of focus of the camera was about 10 cm. The region of good illumination, where the beams of the two lights intersected, was considerably larger than the region which could be traversed by unscattered particles.

The clearing field was supplied by grounding alternate plates and applying a negative potential to the others. Thin sheets of metal (the upper one, 0.02 cm of Al) were placed against the glass walls at the top and bottom of the chamber to provide electrodes for the clearing fields in the extreme upper and lower sections. To simplify the connections the same potential was used across these large sections as was used between the plates. In order to keep the large sections clear of background fog it was necessary to use 65 volts, which gave a higher field strength than necessary between the

plates. The only observable result of this high field was a wide separation of the positive and negative ions, making tracks with an appreciable horizontal component appear double. This separation of positive and negative ions provided a useful time scale. The separation was always the same for the tracks of particles which triggered the cloud chamber. A particle which passed through just before or after the chamber was triggered produced a track in which the separation was smaller or larger, respectively, than the separation of "counter-controlled" tracks. Therefore, in cases where the separation of positive and negative ions could be observed, it was possible to judge whether or not the particle in question arrived simultaneously with the triggering of the chamber.

The camera, cloud chamber, and counters were all fixed rigidly to a frame which could be rotated about an axis parallel to the axis of the chamber and could be clamped solidly at any angle up to $60^{\circ}$ from the vertical.

## 2.2 Method of Triggering.

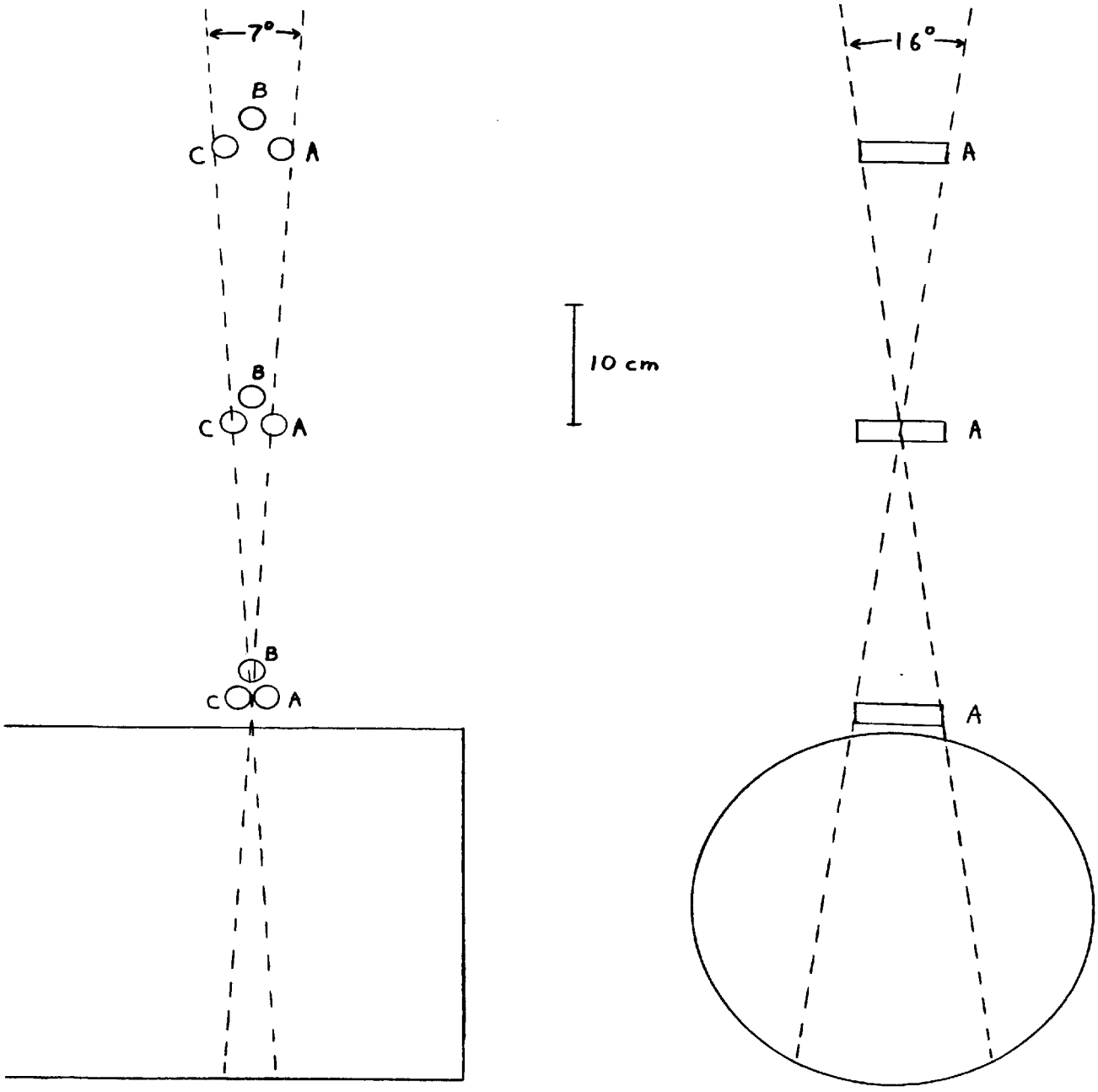
The cloud chamber was triggered by an array of nine Victoreen 1B85 counters. These counters are made of aluminum and have an active length of 6.4 cm, a diameter of 1.9 cm and a wall thickness of 0.030 gm $cm^{-2}$. In order to keep the beam defined by the counters as close as possible to the

focal plane of the camera, the counters were placed with their axes parallel to the front of the chamber and were arranged as indicated in Figure 2. Counters A were connected to one triple-coincidence circuit, counters B to another, and counters C to a third. The pulses were fed directly to the grids of the coincidence tubes, giving an effective resolving time of about 35 microseconds. The outputs of the three coincidence circuits were fed through a cathode-follower mixing stage to the control circuit.

The distance between the top and bottom counters was 45.8 cm. The counters defined a beam with maximum included angles of 16° in the plane parallel to the front of the chamber and 7° in the plane parallel to the axis of the chamber. The counters were mounted in a wooden framework, all of which was well outside of the beam. They were operated at 900 volts, and all of them gave pulses of approximately the same size.

The control circuit provided automatic operation so that when everything was working properly the only required supervision of the apparatus consisted of keeping the expansion ratio in good adjustment and changing the film when necessary. When a triggering pulse entered the control circuit it fired a thyratron which operated several relays, expanding the cloud chamber and shorting out the clearing field as rapidly as possible. The camera shutter was opened immediately and the flash tubes were fired after an electronic delay of about 0.08

Fig. 2. Arrangement of Counters




A. Side View

B. Front View

second which permitted the drops to grow to suitable size. During the two minute recycling period, controlled by a clock motor driving cams, two slow expansions were made and the film was advanced.

Two mechanical registers were placed so that they would show in the corner of each photograph. One served to number the exposures consecutively. The other, driven by a 10 rpm clock motor, recorded the total elapsed time during which the control circuit was sensitive to triggering pulses. This motor was turned off automatically during each recycling period and whenever the circuit was set for manual operation.

## 2.3 Experimental Conditions

At Ann Arbor the apparatus was operated in a wooden structure on the roof of the Randall Laboratory. In order to reduce the effects of scattering and the number of electrons produced by the materialization of photons, a slot was cut in the roof above the counters and was covered with 0.09 cm of aluminum. The slot was at least 4 cm wider than the beam defined by the counters. It extended across the roof and down the wall, permitting the apparatus to be used at zenith angles up to 60°.

At Echo Lake and Mt. Evans (both in Colorado) the experiments were performed in wooden buildings beneath slots or holes covered with 0.05 cm of aluminum. At each location the

temperature inside the building was controlled thermostatically to within about 1° F. At each of the three locations measurements were made at zenith angles of 0°, 45°, and 60°. At Ann Arbor the apparatus was tilted toward the east, at Echo Lake toward the north, and at Mt. Evans toward the southeast. These directions were determined by the shapes of the buildings used. At each position of the apparatus between 1500 and 2000 photographs were taken.

The altitude of Ann Arbor is 280 meters, at Echo Lake 3260 meters, and at Mt. Evans 4300 meters. According to the I.C.A.N. Standard Atmosphere (3) these altitudes correspond to depths from the top of the atmosphere of 1000, 690, and 605 gm $cm^{-2}$. For greater accuracy the depths should be obtained from the barometric pressures during the times of observation, but for present purposes exact values are not important.

## CHAPTER III

## INTERPRETATION OF DATA

### 3.1 Analysis of the Photographs

The negative of each photograph was examined by means of a stereoscopic viewer. The viewer was made with two lenses (focal length 8 cm) and two prisms to invert the images and thus prevent the cloud chamber from appearing inside out.

Those pictures in which conditions were not suitable for the formation of tracks in all sections of the chamber were rejected. The only exception was a series taken at $0^{o}$ on Mt. Evans, in which the uppermost section of the chamber showed an excessive amount of fog but conditions were good in the rest of the chamber. Several hundred pictures were taken before it was possible to eliminate the condition, which was apparently caused by unequal temperatures. In these pictures particles penetrating the top plate were counted, but no attempt was made to count those stopping in the top plate.

The decision on whether or not to reject a picture because of poor track formation was made by examining the amount of background fog rather than the tracks themselves. This method avoids discriminating in favor of long and easily seen tracks. In general the rejected pictures occurred not

singly but in groups, taken during times when the expansion ratio had drifted away from proper adjustment or moisture had condensed on the front glass. In such cases it was only necessary to determine the beginning of the group to be rejected. The end of the rejected group was reached at the point where the fault was corrected. Thus, most of the rejected pictures were, in effect, chosen at random, and their rejection could not have introduced any bias tending to favor one type of event over another.

Each of the acceptable pictures was examined carefully and assigned to one of the following classifications, which are discussed in the succeeding paragraphs:

A. Blank pictures
B. Side showers
C. Extraneous single particles
D. Penetrating particles
E. Stopped heavy particles
F. Low energy electrons
G. High energy electrons
H. Multiple electrons

A. The blank pictures include all those in which there are no tracks of the right age to have been made coincidentally with the triggering of the counters. This group includes all particles which penetrate the counters but have insufficient energy to penetrate the glass wall of the cloud chamber. It also includes electrons of low energy which are scattered in the glass through sufficiently large angles so that they are not observed to come out into the chamber. A small frac-

tion of the events in this group are caused by random coincidences of unassociated counts and some are caused by diffuse air showers in which the counters were triggered but no particles passed through the visible part of the chamber.

The age of a track can be judged by comparing its diffuseness with that of tracks known to be "counter-controlled", and also, if possible by observing the separation of positive and negative ions (see Section 2.1). It is not necessary to measure the diffuseness or the separation of the ions with very high accuracy because, in selecting which tracks are acceptable, not only the age but also the spatial position is considered. It is very improbable that a particle which passes through the chamber slightly before or after the counters are triggered will also have an acceptable position. From now on it is assumed that all particles and tracks to which reference is made are of "counter-controlled" age.

B. Side showers include all events in which two or more particles enter the chamber from a direction other than that defined by the counters. These events may be caused either by air showers or by locally-produced showers generated in the roof or in other material near the apparatus.

C. Extraneous single particles include all single particles which do not emerge from the chamber wall within the allowed area beneath the counters and also penetrating particles and

Fig. 3 Typical Photographs



A. Penetrating particle



B. Penetrating particle



C. Side shower



D. Stopped proton

Fig. 4 Typical Photographs



A. Low energy electron



B. High energy electron



C. Medium energy electron



D. Multiple electrons

energetic electrons which enter through the allowed area but do not have the right direction. (The allowed area is defined by assuming that there is no scattering in the counters. When the pictures are viewed stereoscopically the boundaries of this area can be estimated with the aid of the four vertical wires on the top plate.) Some of these extraneous particles originate from events of the same types that produce the side showers. Others are due to events in which a particle produces a secondary electron in the roof or in one of the counters and the original particle triggers some of the counters while the secondary triggers the others.

D. Penetrating particles, for present purposes, are defined as particles which penetrate all the absorbing plates without producing showers in the lead and therefore are presumably heavier than electrons. A penetrating particle, in traversing the lead plates, frequently produces one or more collision electrons of low energy, but such events can easily be distinguished from electron-induced showers by the fact that the heavy particle continues on its way without appreciable scattering. In a few cases an energetic secondary electron is produced and starts a small shower, but even in such cases the undeviated track of the penetrating particle can generally be distinguished. (See Fig.3B)

E. A heavy particle that stops in one of the plates can be distinguished from an electron by the fact that its ionization is greater than twice the minimum value. An electron of low enough energy to produce the same ionization will make an irregular track due to scattering in the gas and if it has already penetrated one or more plates the upper segments of the track will show minimum ionization. Table I shows the expected ionization for protons and mesons of various residual ranges, calculated from the data given by Gross (16) for range as a

function of momentum and by Rossi and Greisen (34) for collision loss as a function of momentum. The rest energy of the meson was taken as 107 Mev. It was anticipated that by means of this information it would be possible to distinguish between mesons and protons. However, it turned out that in many cases it was possible to determine only that the ionization was several times minimum. The tracks were not sufficiently diffuse to permit accurate counting of drops in a dense track and often there was too much background to permit counting even in a track of low density. Since the numbers of positively identified protons and mesons are too small to be significant statistically, they have not been listed separately.

Table I

IONIZATION OF SLOW PROTONS AND MESONS IN UNITS OF MINIMUM IONIZATION

| Residual Range | | Proton | Meson |
|---|---|---|---|
| 1 Pb plate | - 7.2 gm cm$^{-2}$ | ~6 | 2.3 |
| 2 Pb plates | - 14.4 " " | 4.4 | 1.8 |
| 3 " " | - 21.6 " " | 3.6 | 1.6 |
| 4 " " | - 28.8 " " | 3.2 | 1.4 |
| 1 Brass pl. | - 5.5 " " | 5.5 | 2.2 |
| 1 Al pl. | - 1.7 " " | | 3.4 |
| 2 Al | - 3.4 " " | ~7.5 | 2.5 |
| 1 Pb + 1 Br | | 4.4 | 1.7 |
| 1 Br + 2 Al | | 4.5 | 1.4 |

F. Low energy electrons are those stopping in one of the first four plates. Each of these was listed according to the plate in which it stopped, and was counted even when it emerged from the top wall of the chamber in a direction different from that defined by the counters. According to Rossi and Greisen (34) the RMS angle of deflection due to multiple scattering when a

particle traverses a plate of thickness x is given by $\theta = \frac{21}{cp\beta}\sqrt{\frac{x}{X_o}}$, where p is the momentum in Mev/c and $X_o$ is the radiation length of the material in the plate, defined by $(\frac{4N_o}{137\ A} Z^2 r_o^2 \log 183\ Z^{-1/3})^{-1}$. The energy loss in the plate is neglected. $cp\beta$ is equal to the energy of the particle for energies much larger than the rest energy. For the top wall of the cloud chamber, x = 1.57 gm $cm^{-2}$ and $X_o$ = 30.8 gm $cm^{-2}$, giving $\theta = 4.7/cp\beta$. Thus an electron of 30 Mev, which is about the upper limit of energy for stopping in the brass plate, will have an RMS deflection of 9°. The second Al plate corresponds to a maximum of about 10 Mev, giving $\theta$= 27° as a lower limit. Similarly, the minimum RMS deflection for electrons stopping in the first plate is 39°. Actually, the energy loss in the glass (about 4 Mev) is not negligible and the correct values of $\theta$ are somewhat larger. Since the angular distribution of monoenergetic particles is Gaussian when energy loss is neglected (34), approximately 5% of the particles are deflected by more than twice the RMS value. It is estimated that an appreciable number of electrons may be missed if they scatter more than about 60° in the glass. Therefore, scattering in the glass causes no serious errors in the number of electrons penetrating the first two plates, but does cause a small error in the number observed to stop in the second plate and a larger error in the number observed to stop in the first plate. Electrons which entered at angles much larger than the expected RMS value were recorded as questionable.

High energy electrons include all those penetrating the first four plates. A considerable number of these merely

stopped in the first lead plate. Others had sufficient energy to penetrate several lead plates, generally with some multiplication. Those with very high energies started large showers in the lead. For each of these electrons the total number of track segments beneath the brass plate and beneath each of the lead plates was recorded. (A track segment is a section of track extending between two plates or between the lowest plate and the bottom of the chamber.) In cases where a particle hit the upper surface of a lead plate and was obviously scattered back out of the plate it was counted only once. In doubtful cases such particles were frequently counted twice.

H. Multiple electrons occurred when air showers were incident in the direction defined by the counters. Generally in such cases several electrons entered the cloud chamber within the allowed area. Even if scattering in the glass is assumed to be negligible it is difficult to measure directions of tracks with sufficient accuracy to be sure whether or not the particles came through all the counters. Therefore the best that can be done in counting these electrons is to set an upper limit by including all those that look as though they might be allowable. Furthermore, there were usually many electrons entering outside the allowed region and, after passing through the first plate they could not be distinguished from those that were counted. Therefore it was not possible to obtain any information concerning the energies of those that were counted. Fortunately, the number of electrons occurring multiply turned out to be a relatively small fraction of all the electrons observed.

Not more than ten events were observed in which two allowable electrons entered the chamber unaccompanied by other particles. In these cases both were counted.

3.2 Nature of the Penetrating Particles.

The total amount of absorbing material through which the penetrating particles had to pass is 1.6 gm $cm^{-2}$ of Pyrex plus 4.7 gm $cm^{-2}$ of aluminum plus 5.6 gm $cm^{-2}$ of brass plus 29.0 gm $cm^{-2}$ of lead. Assuming a rest energy of 107 Mev and using the curves given by Rossi (37), it is found that for $\mu$-mesons this amount of material corresponds to a lower limit of momentum of 150 Mev/c and is equivalent to a residual range in air of 23 gm $cm^{-2}$. For protons, with rest energy 937 Mev, the corresponding limit of momentum is approximately 600 Mev/c. According to Mylroi and Wilson (27) the vertical intensity of protons with cp > 1000 Mev is $0.55 \times 10^{-4}$ $cm^{-2}$ $sec^{-1}$ $sterad^{-1}$ at sea level, and can be considered to increase exponentially with altitude, with an absorption length L = 143 ± 13 gm $cm^{-2}$. The number between 600 and 1000 Mev is very small compared to the number above 1000 Mev. The total vertical intensity of penetrating particles at Ann Arbor (30 gm $cm^{-2}$ above sea level) is 0.0090 $cm^{-2}$ $sec^{-1}$ $sterad^{-1}$ (see Section 6.1) and it follows that about 0.75% of these particles are protons. Taking L = 143 gm $cm^{-2}$, the vertical intensity of protons at Mt. Evans is 16 times that at Ann Arbor. The vertical intensity of penetrating particles is 2.1 times that at Ann Arbor (Section 6.1), and therefore 5.7% of the penetrating particles are protons. This figure increases to 7.5% if L is taken as

130 gm $cm^{-2}$. The exact variation of the proton intensity with zenith angle is not known, but it is probable that the proportion of protons in the penetrating component decreases with increasing zenith angle.

At the altitudes of this experiment it is not likely that there are many particles other than $\mu$-mesons and protons in the penetrating component. The only other particles that might be present in significant quantities are $\pi$-mesons. The number of $\pi$-mesons is depleted both by nuclear interactions and by decay (lifetime = $10^{-8}$ sec), while the number of protons is depleted only by nuclear interactions. The number of $\pi$-mesons produced may be greater than that of protons, but not by a very large factor. Thus, it may be expected that the number of $\pi$-mesons traversing the apparatus is small compared to the number of protons.

## 3.3 Energy Calibration for Electrons of Low Energy.

A charged particle, in passing through matter, loses energy both by ionization (collision loss) and by radiation. The ionization process involves a large number of interactions in each of which a small amount of energy is transferred, and consequently the fluctuations in the amount of energy lost per unit path length are very small. The radiation process, on the other hand, involves relatively few interactions in each of which a large amount of energy may be transferred, and the fluctuations are large. Thus, if the initial energy of a particle is to be a well defined function of the range, the rate of energy loss by ionization must be large compared

to the rate of energy loss by radiation. For electrons this condition is fulfilled only in materials of small atomic number and at rather low energies. When this condition is fulfilled, the total energy loss of an electron may be defined as the sum of the collision loss and the average radiation loss, and the range may be calculated as a function of energy from the total energy loss. It will then be a good approximation to assume that every electron of given initial energy travels a distance given by the corresponding range, and thus the energy can be determined from the range. The approximation becomes less good as the energy of the electron or the atomic number of the absorbing material is increased. The situation is further complicated by the effect of multiple scattering, which makes it difficult to predict what thickness of absorber an electron will penetrate even if its total range is known.

The first three plates in the cloud chamber were made of aluminum because that is the material of lowest atomic number that was readily available. The fourth plate was made of brass because the energy loss per centimeter is larger in brass than in aluminum and it seemed desirable to obtain a point on the energy spectrum corresponding to a higher energy than would have been obtained with another aluminum plate. This was possibly a mistake since the energy corresponding to a given thickness is less well defined in brass than in aluminum.

For a relativistic electron of total energy E, traversing a material of atomic number Z and atomic weight A, the energy loss by collision (18) is given by - -

$$-\frac{dE}{dx} = 0.1535 \frac{Z}{A} (3 \log E - 2 \log Z + 22.4) \text{ Mev gm}^{-1} \text{ cm}^2 \quad (1$$

Here, the average energy of ionization, IZ, has been approximated by taking I = 11.5 ev, as suggested by Wilson (47). Multiplying by the density of the material gives the collision loss in Mev/cm. If the material is composed of more than one element the energy losses in Mev $gm^{-1}$ $cm^2$ must be combined according to the proportions by weight of the respective elements.

In calculating the average radiation loss for the present experiment it was desired to take into account the fact that, when an electron transfers most of its energy to a photon, the photon can materialize in one of the lead plates below, making one or more observable electrons. In such cases (very few were observed) the electron was counted as having emerged from the plate in which it radiated and as having traveled a further distance which was estimated by observing the secondary electrons. A rough estimate indicates that a 20 Mev photon passing vertically through the lead plates would have a probability somewhat larger than 0.5 of producing an observable secondary electron. Therefore, only that part of the radiation loss was counted which involves energy transfers of less than 20 Mev. This means that for an electron of energy $E > Q$, where Q will be taken as 20 Mev, the differential cross section for radiation must be integrated only between photon energies of zero and Q. For $E < Q$, the complete radiation loss, including photons up to energy E is used.

The asymptotic value of the average radiation loss is given by Heitler (18) as $-\frac{dE}{dx} = E Z^2 \frac{N_o r_o^2}{137 A} [4 \log (183 Z^{-1/3}) + 2/9]$.

This expression is good only at very high energies where the hypothesis of complete screening of the nuclear electric field by the atomic electrons is valid. At lower energies the energy loss given by this formula is too large and must be reduced by an amount which can be determined from the curves given by Heitler on page 173 of the above reference. At 5 Mev, the lowest energy considered here, the correction amounts to about 35%.

Radiation can be emitted not only when a moving electron is deflected by a nucleus but also when it is deflected by one of the atomic electrons. The asymptotic cross section for this interaction has been calculated by Wheeler and Lamb (49). Integrating that cross section over all possible photon energies, and adding the result to the expression given above, we find that the total asymptotic radiation loss is given by

$$-\frac{dE}{dx} = E\,\frac{N_o r_o^2}{137\,A}\left[4Z^2 \log\left(183\,Z^{-1/3}\right) + 2\,Z^2/9 + 29.3Z - 2.67\,Z \log Z\right] \qquad (2$$

This expression can be corrected for use at low energies by means of the curves mentioned above. A different correction probably should be used for the last two terms, but since these terms represent a relatively small part of the total value (about 10% for aluminum) the error introduced is not large.

For use in the case $E > Q$, the differential cross sections given by Heitler and by Wheeler and Lamb were integrated over photon energies from zero to Q. Adding the two results gives an energy loss of - -

$$-\frac{dE}{dx} = Q\frac{N_o r_o^2}{137\,A}\left[\frac{4}{3}(4 - 2Q/E + Q^2/E^2)Z^2 \log(183\,Z^{-1/3}) + \frac{2}{9}Z^2(2 - Q/E) + Z(19.6 - \frac{16}{9}\log Z)(2-Q/E) + Z(9.7 - \frac{8}{9}\log Z)\,Q^2/E^2\right] \quad (3$$

To a very good approximation this expression can be represented by using Eq. (2 and replacing E by $(4 - 2Q/E + Q^2/E^2)\,Q/3$.

The calculated values of radiation loss at several energies are given in Table II for duralumin and brass (67% Cu, 33% Zn, density 8.40). Also listed are values of the total energy loss obtained by adding the radiation loss to the collision loss obtained from Eq. (1.

TABLE II

ENERGY LOSS OF ELECTRONS IN ALUMINUM AND BRASS

(In Mev/cm)

| Kinetic Energy | Duralumin 24S | | Brass | |
|---|---|---|---|---|
| | Rad. Loss | Total Loss | Rad. Loss | Total Loss |
| 5 Mev | 0.41 | 5.02 | 2.4 | 14.9 |
| 10 | 0.90 | 5.90 | 5.3 | 18.9 |
| 15 | 1.41 | 6.64 | 8.2 | 22.5 |
| 25 | 1.95 | 7.48 | 11.3 | 26.5 |
| 50 | 2.29 | 8.22 | 13.2 | 29.6 |
| 100 | 2.57 | 8.92 | 14.8 | 32.4 |

In order to convert the total energy loss to range, the integral $I(W) = \int_5^W \frac{dE}{-(dE/dx)}$ was evaluated graphically as a function of W. This gives the distance traveled by an electron from the point at which its energy is W to the point at which its energy is 5 Mev. The range of a 5 Mev electron in aluminum

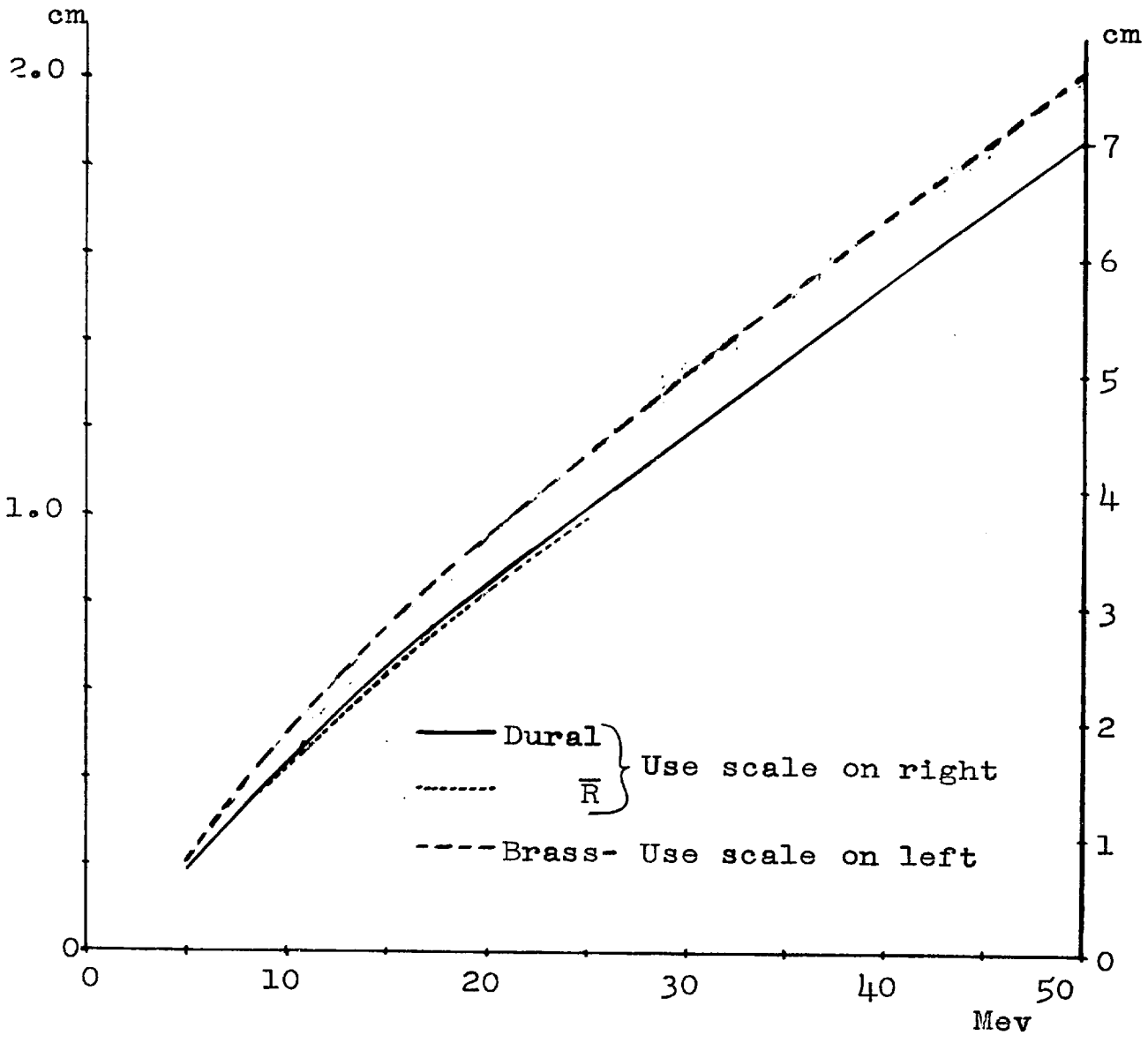
is taken as 0.72 cm, in agreement with the value of average range given by Fowler, Lauritsen, and Lauritsen (10). The maximum range of a 5 Mev electron in copper has been determined experimentally by Hereford and Swann (19) to be 2.5 gm $cm^{-2}$. By comparison with the ratio of average to maximum range at 5 Mev in aluminum, as given by Fowler et al., the average range in brass is taken as 1.7 gm $cm^{-2}$, or 0.20 cm. Thus the range in aluminum is given by I(W) + 0.72 and in brass by I(W) + 0.20. These ranges are plotted as functions of the kinetic energy in Figure 5.

The dotted curve in Figure 5 represents the average range, $\overline{R}$, as given by Fowler et al. This function is derived from a semi-empirical calculation of the effect of multiple scattering. For two reasons the values of range suitable for use in the present experiment might be expected to be somewhat larger than $\overline{R}$. First, in the calculation of $\overline{R}$ it was assumed that all electrons deflected by an angle larger than one radian are lost, whereas electrons deflected by angles up to 90° can be observed in the cloud chamber. Second, the absorption curves (giving the probability that an electron of given energy will penetrate various thicknesses of absorber) from which $\overline{R}$ is calculated indicate that at 5 Mev about half the electrons penetrate a distance equal to $\overline{R}$ but that at higher energies considerably more than half reach $\overline{R}$. As a rough approximation it may be considered that the median range (distance reached by half the electrons) is most suitable for use in the present case. However, the median range, as determined from the absorption curves, is larger than the range given by the

solid line in Fig. 5. Consequently it was decided to use the ranges as given in Fig. 5 without further correction for scattering. The effect of scattering is greatest at very low energies and is partially compensated by the way in which the residual range at 5 Mev is determined. It may be expected that the ranges given for brass are less accurate than those for aluminum because the effects of radiation and scattering are both larger in brass.

Fig. 5

Range-Energy Graph for
Duralumin and Brass



The total energy loss was calculated for Pyrex (assumed to have the composition given in Reference 21) in the same way as for aluminum. At 5 Mev the energy loss per cm in Pyrex is 0.850 times that in aluminum. At 15 Mev the ratio is 0.828, and at 50 Mev it is 0.814. Using 0.83 as an average, we find that the 0.63 cm of Pyrex in the top wall of the cloud chamber is equivalent to 0.52 cm of aluminum.

It can easily be proved that the average path length through the two walls of a cylindrical counter, for particles uniformly distributed in space and moving perpendicular to the axis of the counter, is $\pi d$, where d is the thickness of the counter wall and is assumed to be much smaller than the radius. Making use of this result, and taking into account the overlapping of the lower counters, we find that the average path length through all the counters is 0.12 cm of aluminum. The roof at Ann Arbor was 0.09 cm of aluminum and in Colorado was 0.05 cm. For simplicity, an average value of 0.07 cm will be used. Thus the amount of material which particles must traverse in order to enter the cloud chamber is equivalent to the following thicknesses of aluminum:

| | |
|---|---|
| Roof | .07 cm |
| Counters | .12 |
| Pyrex | .52 |
| Electrode | .02 |
| TOTAL - - - - | .73 cm |

The first absorbing plate consisted of .32 cm of aluminum and .003" of phosphor bronze. By comparing the energy losses in brass and aluminum we find that the bronze is equivalent to .03 cm of aluminum.

Table III gives the total amount of material traversed by electrons in penetrating the various absorbers, and the corresponding energies as determined from the range curves of Fig. 5.

TABLE III

ENERGY REQUIRED TO PENETRATE ABSORBERS

| | Material traversed | Energy Required |
|---|---|---|
| To enter chamber | .73 cm Al | 5.1 Mev |
| To penetrate 1st plate | 1.08 cm Al | 6.9 |
| " " 2nd " | 1.70 | 10.4 |
| " " 3rd " | 2.32 | 14.4 |
| " " 4th " | 2.32 cm Al + .66 cm brass | 30 |

It is difficult to estimate the accuracy of this range-energy calibration. A more accurate calibration could be made if more experimental results were available concerning the penetration of electrons through absorbers. It appears that experiments of this type have always been performed in such a way that the electrons are considered as lost whenever they scatter through a small angle. If the penetration probabilities were known for a wide-angle geometry, it would be possible to develop a relation which would give the energy distribution of the electrons in terms of the observed distribution of ranges. However, the relationship would depend on the energy distribution of the electrons being measured and therefore would have to be calculated by a method of successive approximations.

## 3.4 Energy Calibration for Electrons of High Energy

The average development of a shower produced by an electron of given energy can, in principle, be derived from the shower theory when the effects of multiple scattering are neglected. The average numbers of electrons and photons as functions of energy and depth are given by the solutions to two simultaneous integral-differential equations which involve the cross sections for the various interactions by which electrons and photons lose energy. For showers in lead, these equations have only been solved approximately, by the use of simplified expressions for the cross sections (34, 44, 2).

The Monte Carlo method, developed by R. R. Wilson (48), represents a different approach to the problem. This method involves the construction of hypothetical showers in which the individual interactions of radiation and pair production are determined by means of a wheel of chance. The average development of a shower can be determined from a large number of hypothetical showers, each initiated in the same way. The great advantage of this method is that accurate values of the cross sections may be used without the necessity of making approximations. The effect of multiple scattering has been included by assuming that electrons with energy greater than a critical value, $E_r$, are not scattered, and that the motion of electrons of energy less than $E_r$ is completely random. According to Wilson, the number of electrons at a given depth with energy greater than $E_r$, which he calls $n_{st}$, is the same as the number that will be observed emerging from the corresponding lead plate in a cloud chamber when only those emerging near the

shower axis and within 30° of the original direction are counted. Curves of $n_{st}$ as a function of depth are given for initiating energies of 50, 100, 200, 300, and 500 Mev. Wilson also indicates a method of obtaining $n_c$, the number observed when all electron paths between successive lead plates are counted. The electrons counted in the present experiment are essentially those scattered by less than 90°, and the number should be approximately halfway between $n_{st}$ and $n_c$.

A common way of estimating the initiating energy of a shower is to count the number of electrons at the maximum of the shower and compare this number with theoretical predictions of the average behavior of showers. This method makes no use of information which might be derived from observation of the shower at points other than the maximum, but it does avoid errors due to fluctuations in the position of the maximum. The method is satisfactory for very high initiating energies but is not suitable for energies where the maximum number of electrons is small and therefore is subject to large fluctuations. The Monte Carlo curves indicate that at 200 Mev the maximum value of $n_{st}$ is about 2.

The ideal quantity to observe would be the area under the curve giving the number of electrons of all energies as a function of depth. If the effect of scattering is neglected, this area is proportional to the total track length (the total distance traveled by all the electrons). If the ionization loss is assumed independent of energy, the total track length is proportional to the initiating energy. Of course, the area under the shower curve cannot be determined exactly by experi-

mental methods. However, the integral from zero to a depth corresponding to the total amount of absorber present can be approximated by adding together the number of electrons observed in each of the spaces between the plates. The number obtained in this way is related to the initiating energy. It is subject to statistical fluctuations because (a) the assumptions mentioned above are not completely justified, (b) the ordinate of the curve is measured at only a few points, (c) the amount of lead in the cloud chamber is not necessarily sufficient to absorb the whole shower and therefore the number of electrons observed is affected by variations in the distance covered by the shower. There has been no attempt to make a quantitative estimate of these fluctuations. If they are large, the energy spectrum determined by this method will indicate too many electrons of high energy.

On the curves relating to the Monte Carlo calculations, the depths are given in radiation lengths, as is customary in the shower theory. The radiation length, $X_o$, is defined in such a way that for an electron of very large energy, E, the average rate of radiation loss is given by $E/X_o$. The lead plates in the cloud chamber are each equivalent to 1.23 $X_o$, where $X_o$ is taken as .519 cm (31). The material above the lead is approximately equal to 0.42 $X_o$ of brass and 0.24 $X_o$ of aluminum. It is impossible to say that this material is exactly equivalent to any given amount of lead, but for present purposes it will be considered as equivalent to 0.5 $X_o$ of lead. The exact value used is not important since it is small compared to the total amount of lead in the chamber. Thus,

the spaces beneath the brass plate and beneath each of the lead plates correspond to depths of 0.5, 1.7, 2.9, 4.1, and 5.3 radiation lengths. The ordinates corresponding to these five depths were obtained from the Monte Carlo data and were added together. The results for $n_{st}$ and $n_c$ are given in Fig. 6 as functions of initiating energy. A curve is drawn halfway between the points representing $n_{st}$ and the points representing $n_c$. It is assumed that this curve represents the total number of track segments observed moving downward beneath the brass plate and each of the lead plates. The relation between shower size and initiating energy, as derived from Fig. 6 is given in Table IV.

TABLE IV

ENERGIES OF SHOWERS IN THE LEAD PLATES

(A shower of n or more track segments corresponds to a lower energy limit of E Mev)

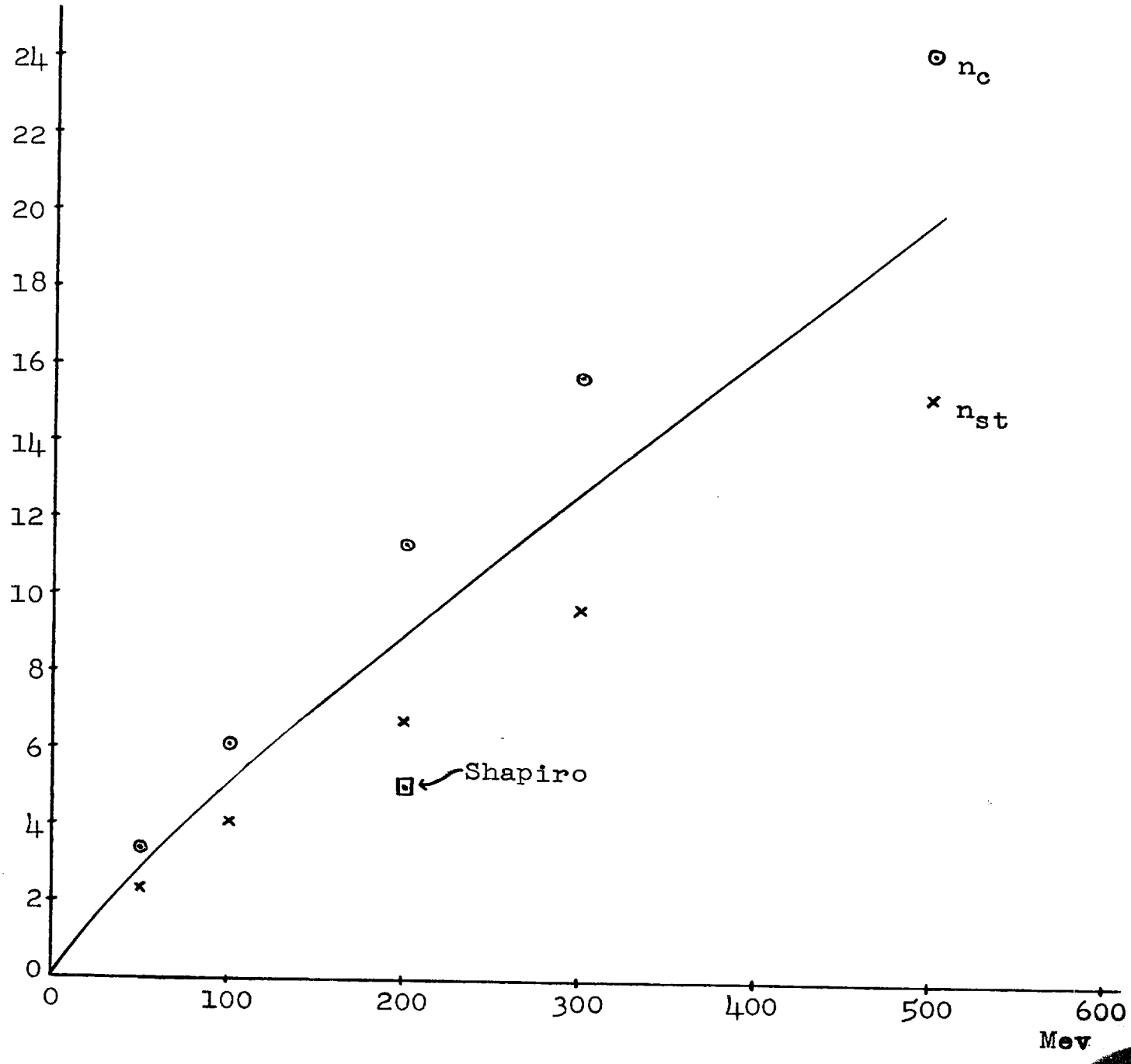
| n | 4 | 6 | 10 | 16 |
|---|---|---|---|---|
| E | 80 | 125 | 230 | 395 |

The point labeled "Shapiro" in Fig. 6 refers to an experiment performed by A. M. Shapiro (42), who used a cloud chamber containing lead plates to observe showers initiated by electrons whose energy was known to be 200 ± 10 Mev. This point was obtained in the way described above from a preliminary curve representing Shapiro's experimental data (43). This point should be lower than the curve because Shapiro excluded electrons scattered through large angles more rigorously than was done in the present experiment. However, the difference seems

larger than might be expected, indicating the possibility that the values of E listed in Table IV are too small. This matter may become clearer when the detailed account of Shapiro's experiment is published.

Fig. 6

Number of Track Segments as Function of Energy



Chapter IV

# EXPERIMENTAL RESULTS AND ERRORS

## 4.1 Observed Numbers of Events

The observed numbers of electrons, classified as described in Chapter III, are listed in Table V. Other types of events are listed in Table VI. For Mt. Evans, the column labeled $0_1^\circ$ gives the pictures obtained while the top section of the cloud chamber was foggy (see Section 3.1) and the column headed $0_2^\circ$ gives the pictures obtained after this condition was corrected. The "Blank pictures" listed under $0_1^\circ$ include all events in which an electron stopped in the top plate. Many of the spaces in Tables V and VI contain two entries. In such cases the smaller number, which is followed by a question mark, refers to events whose identification is not certain. Usually the uncertainty has to do with whether or not the particle actually went through the counters. In other cases the uncertainty is in the age of the track. In a few pictures it is uncertain whether the particle was an electron or a penetrating particle. Such events are listed under the classification which appears most probable.

For completeness, the numbers of nuclear interactions observed in the plates are included in Table VI, although no use is made of the information. Some of these represent events which should have been counted as penetrating particles, but in others the initiating particle came in from the side and one of the secondary particles triggered the counters. The fact that the initiating particle may be a neutron makes it difficult to distinguish between the two cases.

TABLE V NUMBERS OF ELECTRONS OBSERVED

| Description of Electrons | Ann Arbor | | | Echo Lake | | | Mt. Evans | | | |
|---|---|---|---|---|---|---|---|---|---|---|
| | $0^{o}$ | $45^{o}$ | $60^{o}$ | $0^{o}$ | $45^{o}$ | $60^{o}$ | $0^{o}_{1}$ | $0^{o}_{2}$ | $45^{o}$ | $60^{o}$ |
| Producing 16 or more track segments | 12 | 12 | 8<br>2? | 21 | 13 | 10 | 4 | 22<br>2? | 15 | 8 |
| 10 or more | 23 | 20 | 19<br>4? | 37<br>1? | 30 | 23 | 15<br>1? | 49<br>3? | 35<br>1? | 21 |
| 6 or more | 39<br>2? | 37<br>1? | 37<br>5? | 73<br>3? | 55 | 32 | 35<br>1? | 81<br>4? | 64<br>3? | 50 |
| 4 or more | 69<br>4? | 54<br>2? | 51<br>5? | 100<br>6? | 82<br>2? | 57<br>2? | 63<br>3? | 113<br>5? | 98<br>4? | 66<br>1? |
| Penetrating 4th plate | 158<br>8? | 132<br>8? | 128<br>9? | 271<br>11? | 198<br>6? | 147<br>7? | 182<br>6? | 263<br>8? | 243<br>9? | 176<br>2? |
| Penetrating 3rd plate | 248<br>12? | 220<br>10? | 202<br>10? | 396<br>13? | 304<br>9? | 227<br>10? | 284<br>6? | 373<br>9? | 364<br>14? | 273<br>6? |
| Penetrating 2nd plate | 269<br>13? | 253<br>12? | 234<br>11? | 443<br>13? | 342<br>9? | 261<br>12? | 327<br>6? | 408<br>9? | 420<br>15? | 320<br>7? |
| Penetrating 1st plate | 301<br>15? | 294<br>12? | 267<br>15? | 486<br>14? | 402<br>10? | 301<br>14? | 348<br>16? | 435<br>10? | 466<br>15? | 373<br>10? |
| Entering chamber | 323<br>19? | 324<br>18? | 285<br>20? | 504<br>16? | 428<br>14? | 341<br>19? | ---<br>--- | 453<br>12? | 491<br>20? | 398<br>19? |

TABLE VI OTHER EXPERIMENTAL DATA

| | Ann Arbor | | | Echo Lake | | | Mt. Evans | | | |
|---|---|---|---|---|---|---|---|---|---|---|
| | $0^\circ$ | $45^\circ$ | $60^\circ$ | $0^\circ$ | $45^\circ$ | $60^\circ$ | $0^\circ_1$ | $0^\circ_2$ | $45^\circ$ | $60^\circ$ |
| Total acceptable pictures | 1466 | 1625 | 1393 | 1312 | 1463 | 1453 | 878 | 1114 | 1436 | 1443 |
| Blank Pictures | 58 | 83 | 114 | 70 | 119 | 152 | 93 | 67 | 137 | 169 |
| Side Showers | 13 | 30 | 30 | 34 | 84 | 222 | 18 | 27 | 90 | 177 |
| Extraneous single particles | 5 | 37 | 24 | 25 | 19 | 31 | 8 | 20 | 36 | 43 |
| Penetrating particles | 1022<br>2? | 1116<br>3? | 905<br>6? | 622<br>1? | 759<br>1? | 625<br>2? | 349<br>5? | 464<br>8? | 607<br>2? | 579<br>3? |
| Stopped heavy particles | 13 | 9<br>2? | 9 | 19 | 32<br>1? | 56<br>1? | 32 | 34 | 41<br>1? | 47<br>1? |
| Multiple Electrons | 36 | 3 | 0 | 50 | 8 | 0 | 31 | 95 | 19 | 3 |
| Multiple Events | 8 | 1 | 0 | 13 | 2 | 0 | 9 | 20 | 6 | 1 |
| Nuclear Interactions | 3 | 2 | 0 | 8 | 4 | 4 | 10 | 9 | 5 | 6 |
| Events used for counting rate | 1504 | 1275 | 928 | 1549 | 1402 | 760 | 1404 | | 1010 | 892 |
| Total Counting Rate ($min^{-1}$) | .158 | .0664 | .0374 | .400 | .179 | .0946 | .560 | | .288 | .127 |

"Multiple Electrons" gives an upper limit to the number of electrons occurring multiply.
"Multiple Events" gives the number of events in which electrons occur multiply.

In order to indicate the statistical uncertainty of the counting rates, the numbers of events used to determine those rates are listed in Table VI. Events which did not give acceptable pictures are included, but runs during which the mechanism that recorded elapsed time was known not to be working properly are excluded. The mechanism was operated by a synchronous motor which kept good time except when the cam to which it was connected became jammed, in which case the motor stopped. The measurements of elapsed time at Mt. Evans may be in error by a few percent because the AC frequency was not accurately controlled. The data for Ann Arbor $45^{\circ}$ consist of several runs giving counting rates ranging from $0.0612 \pm .0038$ to $0.0693 \pm .0041$. These numbers differ sufficiently to suggest the possibility of a systematic error. The data for the other counting rates exhibit much better internal consistency.

4.2 Errors due to scattering.

Electrons are scattered out of the beam by the material of the roof and the uppermost counters, but these are approximately compensated by those which are scattered in. The compensation would be exact if the directional intensity were isotropic. Although the intensity is not actually isotropic the compensation is still very good because the RMS angle of scattering is only about $10^{\circ}$ for an electron of 10 Mev. No correction has been made for this effect.

The effect of scattering in the bottom counters is negligible. Scattering in the glass wall of the chamber, which has been discussed previously (Section 3.1), is much more important in reducing the observed number of electrons of low

energy. However, the total number of electrons of energy greater than 10 Mev is reduced by an amount that is surely small compared to the statistical uncertainties.

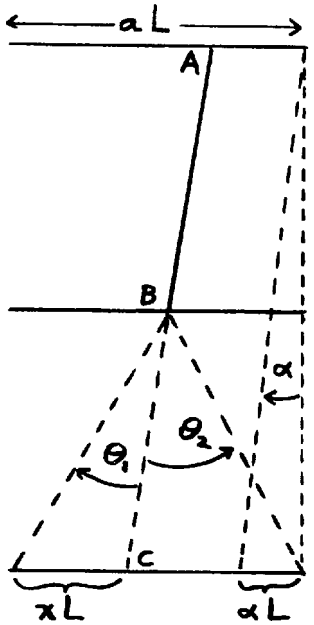
Scattering in the central counters is the most serious source of error. Electrons which should be counted will be eliminated if they are deflected through relatively small angles in such a way that they miss the bottom counters. There will be only partial compensation by others scattered in because only those which come through the top counters can produce coincidences. Comparison of the RMS angle of scattering (Section 3.1) and the angle intercepted by the diameter of one of the bottom counters viewed from the position of the central counters indicates that the two are equal for electron energies of about 10 Mev. Therefore it may be expected that the effect will become negligible only for energies considerably larger than 10 Mev. The importance of this effect was not realized at the time the apparatus was designed. It would have been better to connect the three counters at each level in parallel, making one triple-coincidence telescope of larger included angle.

The effect of scattering in the central counters can be calculated in an approximate way by considering the counters as flat plates of thickness $\pi d$, where d is the thickness of the counter walls. As mentioned previously, $\pi d$ is the average path length through the two walls of a counter for particles distributed uniformly in space and moving perpendicular to the axis of the counter. Therefore, this approximation will give a correction which is too large, because most of the allowed

trajectories of unscattered particles pass through the middle of the center counters where the path length is less than $\pi d$, while many of the trajectories of particles that can be scattered into the beam pass through near the sides where the thickness is greater. The slight overlapping of the three central counters may tend to make the correction too small, but the exact effect is difficult to predict because the extra path length is near the sides of the counters where it is traversed mostly by particles not in allowed trajectories.

The results of the calculation can be expressed in terms of the functions $h_0(x) = \int_x^\infty \exp(-y^2/2)dy$, $h_1(x) = \int_x^\infty h_0(y)dy$ and, $h_2(x) = \int_x^\infty h_1(y)dy$, which are tabulated in the British Association Mathematical Tables (25).

We will consider the scattering projected on a plane perpendicular to the axes of the counters. Let L be the distance between the top and bottom counters and aL the width (diameter) of the counters. An electron which arrives along AB (see accompanying diagram), at an angle $\alpha$ to the axis of the telescope, would strike the bottom counter at the point C, at a distance xL from the edge, if it were not scattered in the central counter. In order to be counted it must be deflected within the limits $\theta_1$ and $\theta_2$. If $a \ll 1$, then $\theta_1 = 2x$, $\theta_2 = 2(a-x)$, and it is permissible to assume that the incident intensity is isotropic. The distribution of scattered monoenergetic particles given by Rossi and Greisen (34)



reduces to $(2\pi)^{-1/2}e^{-u^2/2}du$, where $u = \frac{2E\theta}{21\sqrt{2t}}$, E is the energy in Mev, $\theta$ is the projected angle of scattering, and t is the thickness of the scatterer in units (for aluminum) of 26.3 gm cm$^{-2}$. Therefore the probability that an electron entering along AB will be scattered out is given by

$$(2\pi)^{-1/2}\int_{u_1}^{\infty} e^{-u^2/2}\,du + (2\pi)^{-1/2}\int_{u_2}^{\infty} e^{-u^2/2}\,du ,$$

where $u_1 = Kx$ and $u_2 = K(a - x)$, with $K = \frac{4E}{21\sqrt{2t}}$. In terms of x, the probability is $f(x) = (2\pi)^{-1/2}\left[h_o(Kx) + h_o(Ka-Kx)\right]$. The total number of electrons that are scattered out is proportional to $\int_o^a d\alpha \int_o^{a-\alpha} f(x)dx$. The number of electrons entering along allowed trajectories is $\int_o^a d\alpha \int_o^{a-\alpha} dx = a^2/2$. Therefore the fraction scattered out is given by

$$2/a^2 \int_o^a d\alpha \int_o^{a-\alpha} f(x)dx = 2(Ka)^{-1}(2\pi)^{-1/2}\left[h_1(0) - h_1(Ka)\right] .$$

In a similar way, we can compute the number of electrons which, after entering along trajectories which pass through the top and center counters but do not pass through the bottom counter, are deflected so that they go through the bottom counter. The number of such electrons, in terms of the number entering along allowed trajectories, is given by

$$2(Ka)^{-2}(2\pi)^{-1/2}\left\{Ka\left[h_1(0) - h_1(Ka)\right] - h_2(0) + 2h_2(Ka) - h_2(2Ka)\right\}.$$

Taking the difference between the number scattered out and the number scattered in, we find that the number of electrons counted is reduced by a fraction $F_I = 2(2\pi)^{-1/2}(Ka)^{-2}\left[h_2(0)-2h_2(Ka) - h_2(2Ka)\right] = (\lambda E)^{-2}\left[0.500 - 1.60h_2(\lambda E) + 0.80h_2(\lambda E)\right]$, where $\lambda E = Ka$. In the present case $a = 0.0416$ and $t = 0.030\pi/26.3$, giving $\lambda = 0.0936$.

There will be a small loss due to scattering in the perpendicular plane, past the ends of the counters. Because this effect is small the same calculation can be used, although the assumption of small angles is less accurate. Since the length of the counters is 3.3 times the width, the fractional reduction in this case is $F_2 = .500/(3.3Ka)^2 = .045/(\lambda E)^2$. The other terms are negligible because $h_2(x)$ is a very rapidly decreasing function of x.

Thus the ratio of the number of electrons counted to the number entering along allowed trajectories is $(1-F_1)(1-F_2)$, and the correction factor which should be applied to the observed differential energy distribution is $C(E) = (1-F_1)^{-1}(1-F_2)^{-1}$. The experimental results give the integral distribution, that is the number of electrons of energy greater than E. It can easily be proved that, if $S_0(E)$ is the observed integral distribution, the corrected integral distribution is $S(E) = S_0(E) + \int_E^\infty S_0(E')\frac{dC(E')}{dE'}\,dE'$. In general, the integral must be evaluated graphically or numerically.

Expressed in a form suitable for tabulation, $C(E) = (\lambda E)^2/Y$ and $\frac{dC(E)}{dE} = -\lambda E\frac{2\lambda Z}{Y^2}$, where $X = .545 - .0225/(\lambda E)^2 - 1.60h_2(\lambda E) + .80h_2(2\lambda E)$, $Y = (\lambda E)^2 - X$, and $Z = X - .0225/(\lambda E)^2 - .80\lambda E h_1(\lambda E) + .80\lambda E h_1(2\lambda E)$. Terms which are negligible for $E > 10$ Mev have been omitted.

This correction has been applied to the integral energy spectrum obtained from the present experiment (see Section 6.2). At 10 Mev the correction is about 12%, and at 20 Mev about 4%.

4.3 Other Experimental Errors.

All errors due to inefficiency of the counters and the associated electronic circuits and to possible inaccuracies in the determination of counting rates are eliminated by measuring the intensities of electrons in terms of the intensities of penetrating particles. Accurate values of the latter are known from other experiments (see Section 6.1).

Cosmic ray intensities vary by a few percent in response to meteorological changes in the atmosphere. Measurements at sea level, made by Greisen (15) over a period of four weeks, indicate that the average value of the deviation from the mean is of the order of 1%. The intensities of electrons and of penetrating particles appeared to vary in the same way. Since the present measurements represent averages over period of which the shortest was ten days and the longest was several weeks, the resulting intensities are probably not in error by more than about 1% due to meteorological variations, and the error in the ratios of electrons to penetrating particles is completely negligible.

An electron or penetrating particle which passes through only two counters may generate a secondary electron by collision in the roof or in one of the counters. If the secondary triggers the third counter and one of the two particles enters the cloud chamber with approximately the right direction and position, the event may be counted. Some of the questionable events listed in Tables V and VI are undoubtedly due to events of this kind. Brown, McKay, and Palmatier (6) have studied the production of secondaries by mesons passing through cylindrical aluminum counters of wall thickness 0.11 gm $cm^{-2}$. They

found that the angular distribution can be represented by $\cos^{2.5}\theta$, where $\theta$ is the angle between a secondary and its primary, and that the total number of secondaries which can be detected with counters similar to those used to generate them is of the order of 0.02 per meson. The number produced by electrons should be of the same order of magnitude. The counters used in the present experiment have wall thicknesses of only 0.03 gm $cm^{-2}$ and will cause correspondingly fewer collisions. With thinner walls they can detect a larger proportion of these secondaries which hit them, but this increase is probably smaller than the decrease in the number produced. The amount of aluminum in the roof is roughly the same as was used to generate secondaries in the above experiment. The number of particles passing through two counters and not through the third is a few times the number counted. If 2% of them produce secondaries in the roof or counters, the number of events in which the secondary triggers the third counter will be a fraction of one percent of the number of particles counted, and the number of these events in which a particle enters the chamber in the right place to be counted will be even smaller.

Extra counts may be produced by photons materializing in the roof or in the upper walls of the top counters. The total probability of materialization of an energetic photon (34) is 7/9 per radiation length, which is equal to 0.03 per gm $cm^{-2}$ for aluminum. The roof plus one counter wall is about 0.2 gm $cm^{-2}$, giving 0.006 as the probability for materialization of a photon. The calculations of Richards and Nordheim (31) indicate that, for

large showers in air, the intensity of photons is twice that of electrons for energies greater than 50 Mev, while for energies greater than 5 Mev the ratio is about three. The ratio of the number of electrons of given energy produced in the roof to the number incident is somewhat smaller than indicated by these figures, because the energies of the electrons produced are smaller than those of the photons producing them and the intensity of photons decreases with increasing energy. On the other hand, the effect is increased by the fact that when a photon materializes it produces two electrons, either one of which may trigger the apparatus. Angular deviations of the produced electrons from the direction of the parent photon may be neglected because they are small and therefore are compensated by photons coming from other directions. Thus, we can conclude that between one and two percent of the measured electron intensity may actually consist of photons. This error is small compared to the statistical errors and no correction has been made for it.

Another possible source of error is that a particle which appears to have come through the counter telescope without actually having done so may appear in a picture which is triggered in the same way as those events which cause blank pictures or extraneous single particles. Such a particle might be related to the particles which triggered the counters, or it might occur merely as a random coincidence. (The resolving time for such coincidences is determined by the accuracy with which the ages of tracks can be measured, and therefore is rather long.) Errors of this sort would be greatest for electrons of low

energy, which are considered as allowable even when they enter the chamber at large angles. In order to determine the frequency with which random coincidences of this type occur, about 500 pictures of penetrating particles were examined to see whether they contained allowable electrons. These pictures may be considered as occurring at random with respect to electrons not associated with the particles which triggered the chamber. Only one allowable electron penetrating the first plate was found. Therefore, we may conclude that, for electrons penetrating the first plate, errors due to random coincidences are negligible. Because of the spatial restrictions on an allowable track, the numbers of false events where the observed particle is related to the particle or particles triggering the counters should be only a small fraction of the numbers of blank pictures and extraneous single particles. This fraction should be even smaller at large zenith angles since most particles come from near the vertical direction. Thus it appears unlikely that errors due to particles that did not pass through the telescope could be appreciable compared to the statistical errors.

If the cloud chamber had been triggered by a double-coincidence telescope, as might appear desirable in order to eliminate scattering in the central counters, there would have been a considerable uncertainty in the electron intensities due to events of the type considered above. Some preliminary measurements were made with double-coincidence triggering (at 0° in Ann Arbor). The ratio of blank pictures to penetrating particles was nearly eight times that obtained with triple-coincidence triggering, and the intensities of low energy electrons were

considerably higher. The latter difference was greater than could be explained by the effects of scattering and was undoubtedly due to the inclusion of electrons that did not pass through the counter telescope.

## 4.4 Correction for Finite Angle of Telescope.

If $I d\Omega dA$ represents the number of particles incident per unit time within an element of solid angle $d\Omega$ upon an area dA which is perpendicular to the direction of incidence, then I is called the directional intensity of the particles. The directional intensities of most cosmic ray particles are essentially independent of the azimuthal angle but are strongly dependent on the zenith angle. Therefore the placement of the counters in the present experiment appears unfavorable since the angular opening in the vertical plane is $16^{\circ}$, while in the plane perpendicular to that it is only $7^{\circ}$. Fortunately, it can be proved that the effect on the observed directional intensities is very small.

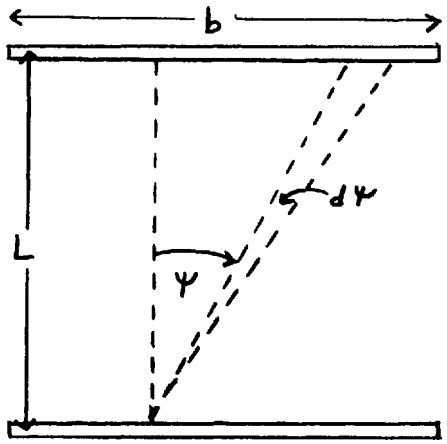
Suppose that a telescope is made from two parallel cylindrical counters, each of a diameter a and length b, separated by a distance L. If L is much larger than a, the counters may be represented by rectangles of width a and length b, lying in planes perpendicular to the axis of the telescope, and variations of intensity across the widths of the counters may be neglected. Then, if $I(\Psi)$ is the directional intensity at an angle $\Psi$ from the axis of the telescope (see accompanying diagram), the counting rate of the telescope is given by - -

$$N = \iint I(\Psi) d\Omega dA = (a/L) \int I(\Psi) \cos\Psi d\Psi dA.$$

If the angle $\alpha$ is defined by $\tan\alpha = b/L$, then $\psi$ varies from $-\alpha$ to $\alpha$ and it can be shown that - -

$$N = a^2 \int_{-\alpha}^{\alpha} (\tan\alpha - |\tan\psi|)\cos^2\psi I(\psi)d\psi$$
$$= 2a^2 \int_{0}^{\alpha} (\tan\alpha - \tan\psi)\cos^2\psi I_e(\psi)d\psi,$$

where $I_e(\psi)$ is the even part of $I(\psi)$.




Suppose the axis of the telescope is tilted at an angle $\theta$ from the vertical, with the axis of the counters lying in a vertical plane, and suppose that the directional intensity of the particles being observed is given by $I(\theta) = I_o\cos^n\theta$, where $I_o$ is the vertical intensity. Then $I(\psi) = I_o\cos^n(\theta + \psi)$, and it can be proved by expanding in powers of $\psi$ and $\alpha$ that the counting rate is equal to

$$N(\theta) = I(\theta)a^2\alpha^2 (1 + C\alpha^2 + \ldots),$$

where $C = 1/3 - n/12 + \left[n(n-1)/12\right] \tan^2\theta$. The succeeding terms involve higher powers of $\alpha$ and may be neglected when $\alpha$ is small.

The telescope used in the present experiment consisted of three independent sets of counters and therefore the ratio of counting rate to directional intensity is $3a^2\alpha^2(1 + C\alpha^2)$. The measured values of a and $\alpha$ are 1.9 cm and 0.14 radian, giving $3a^2\alpha^2 = 0.21$ cm$^2$sterad. This figure is only approximate since the effective lengths of the counters were not determined very accurately. Thus, the directional intensities are given by $I(\theta) = N(\theta)/0.21(1 + C\alpha^2)$.

Values of $C\alpha^2$ are listed in Table VII for n = 2.1 (for mesons) and n = 3 (approximate for electrons).

TABLE VII

CORRECTION FACTORS FOR OBTAINING DIRECTIONAL INTENSITY FROM COUNTING RATES

| $\theta$ | $C\alpha^2$ for n = 2.1 | $C\alpha^2$ for n = 3 |
|---|---|---|
| 0° | 0.003 | 0.002 |
| 45° | 0.007 | 0.011 |
| 60° | 0.014 | 0.031 |

## Chapter V

## CALCULATION OF NUMBER OF ELECTRONS PRODUCED BY MESONS

### 5.1 Previous Calculations.

Rossi and Greisen (35) have developed a method for calculating the intensity of electrons of all energies resulting from the decay of μ-mesons. This method is based on the following assumptions: (a) The decay electron is assumed to have a unique energy in the rest system of the meson. (b) Variations with altitude in the shape of the energy spectrum of mesons are neglected. (c) The depth in the atmosphere at which the electrons are observed is assumed to be greater than the maximum penetration of showers. (d) The problem is considered as one-dimensional, scattering and other angular deviations being neglected. The rate of dissipation of energy by electrons, rather than the intensity, is the quantity actually calculated. The two are proportional if the ionization loss is considered as constant. It is shown that the energy dissipated by electrons at depth x is equal to the energy going into the electron component at depth $(x - \bar{x})$, where $\bar{x}$ is the average range of the showers initiated by the decay electrons (averaged over the energies of the decay electrons and of the mesons) and is equal to 3.04 radiation lengths for fast mesons ($pc > 300$ Mev). Rossi and Klapman (36) made further calculations to find the number of electrons of energy greater than 10 Mev resulting from the decay of mesons, under the assumption that this number is affected by the variation in rate of production of decay electrons with altitude in the same way as is the number of electrons of all energies. The same authors also determined the number of electrons of energy

greater than 10 Mev resulting from collision processes of mesons.

It is now known that the decay electron does not have a unique energy in the rest system of the meson and that, consequently, the distribution of energies in the laboratory system is very different from that used in the calculations mentioned above. It appeared that a calculation taking into account the correct energy distribution might yield results of significantly greater accuracy. It was found that a calculation of this sort is feasible, although rather lengthy. Three successive integrations are required, of which only the first can be carried out analytically. This method has the additional advantage that it is not necessary to assume a constant shape for the meson spectrum. The problem is considered as one-dimensional, and the procedure is described in the next section.

## 5.2 A More Accurate Method of Calculation.

In the rest system of the meson, let $\theta$ represent the angle between the direction of motion of the electron and the direction determined by the motion of the meson, let u represent the total energy of the electron, and let the distribution of energies be given by $F(u)du$, where $\int_0^{u_m} F(u)du = 1$. $u_m$ is the maximum energy of the electron and is equal to one half the rest energy of the meson. Then, since all directions are equally probable for the electron, the probability that it will have an energy between u and $u + du$ and a direction between $\theta$ and $\theta + d\theta$ is $\frac{1}{2}\sin\theta\, F(u)du d\theta$.

In the laboratory system, let the energy of the electron be U and let the angle between the directions of the electron

and meson be $\psi$. Let P represent the momentum of the meson multiplied by $c/\mu$, where $\mu$ is the rest energy. Then P may be called the "reduced momentum" and is equal to $\beta/\sqrt{1-\beta^2}$.

It follows from the Lorentz transformation that

$$U = u\sqrt{P^2+1} + P\sqrt{u^2-\nu^2}\cos\theta \qquad (1$$

and

$$u = U\sqrt{P^2+1} - P\sqrt{u^2-\nu^2}\cos\psi, \qquad (2$$

where $\nu$ is the rest energy of the electron and is negligible for electron energies larger than about 5 Mev. Assuming that $\psi$ must lie between $0^\circ$ and $90^\circ$, it is apparent from Equation 2 that, for given values of U and P, u must lie between

$$u_1 = U\sqrt{P^2+1} - P\sqrt{u^2-\nu^2} \cong U(\sqrt{P^2+1} - P) \qquad (3$$

and

$$u_2 = U\sqrt{P^2+1} \qquad (4$$

Actually, $\psi$ is very small for most of the electrons and $u_2$ can be taken equal to $u_m$ without introducing any appreciable error.

The independent variables u and $\theta$ can be transformed to u and $\psi$ by making use of Equation 1. The Jacobian of this transformation is equal to $P\sqrt{u^2-\nu^2}\sin\theta$ and therefore $dudU = P\sqrt{u^2-\nu^2}\sin\theta\, dud\theta$. Consequently, $\frac{1}{2}\sin\theta\, F(u)dud\theta$ transforms to $\frac{F(u)dudU}{2P\sqrt{u^2-\nu^2}}$. Thus the probability that the electron will have energy between U and dU is given by $P^{-1}g(U,P)dU$, where

$$g(U,P) = \int_{u_1}^{u_2} \frac{F(u)du}{2\sqrt{u^2-\nu^2}}. \qquad (5$$

Let $M(h,P)$ represent the intensity of mesons between P and P+dP observed at a depth h below the top of the atmosphere, where h is measured in gm $cm^{-2}$. If $\tau$ is the mean lifetime in the rest system, then the fraction of the mesons which decay in a time dt, measured in the laboratory system, is $\tau^{-1}\sqrt{1-\beta^2}\,dt$. In a time dt, a meson travels through a depth $dh = c\beta\rho(h)dt$, where $\rho(h)$ is the density of the atmosphere. Therefore the

number of mesons decaying between h and h+dh per unit time is $\frac{\sqrt{1-\beta^2}\ dh}{\tau c \beta \varsigma(h)} M(h,P)dP = \frac{M(h,P)dPdh}{Pc\tau\varsigma(h)}$ .

It follows that the intensity of decay electrons of energy between U and U+dU produced between h and h+dh is

$$G(U,h)dUdh = \frac{dUdh}{c\tau\varsigma(h)} \int_0^\infty p^{-2} g(U,P)M(h,P)dP \qquad (6$$

Let $N(U,E,s)$ be the average number of electrons of energy greater than E, at depth h, produced by one electron of energy U at depth h-s. Approximations to this function can be obtained from the shower theory.

The intensity of electrons of energy greater than E observed at depth h is then given by

$$S(h,E) = \int_E^\infty dU \int_0^h ds\ N(U,E,s)G(U,h-s) \qquad (7$$

To evaluate this double integral would require a large amount of labor which is not worth while because the function N(U,E,s) is not known very accurately for values of E other than zero. A function which has been calculated with much greater precision is the integral track length, which is defined by

$$Z(U,E) = \int_0^\infty N(U,E,s)ds.$$

Considering the integral over s in Equation 6 and expanding G(U,h-s) in a Taylor series, we have

$$\int_0^h N(U,E,s)\left[G(U,h) - s\frac{\partial G(U,h)}{\partial h} + \frac{s^2}{2}\frac{\partial^2 G(U,h)}{\partial h^2} + \cdots\right]ds$$

The upper limit can be changed to infinity because no decay electrons are produced above the top of the atmosphere and therefore G(U,h-s) = 0 for s > h. The expression then becomes

$$Z(U,E)\left[G(U,h) - \bar{h}\frac{\partial G}{\partial h} + \frac{\bar{h^2}}{2}\frac{\partial^2 G}{\partial h^2} + \cdots\right]$$
$$= Z(U,E)G(U,h-\bar{h}) + \frac{1}{2}Z(U,E)\left[\bar{h^2} - (\bar{h})^2\right]\frac{\partial^2 G(E,h)}{\partial h^2} + \cdots ,$$

where $\bar{h} = Z^{-1}\int_0^\infty sN(U,E,s)ds$ and $\overline{h^2} = Z^{-1}\int_0^\infty s^2N(U,E,s)ds$ .
In terms of quantities defined by Rossi and Greisen (34), $\bar{h} = X_o\bar{t}_\pi$ and $\overline{h^2} - (\bar{h})^2 = X_o^2\tau_\pi^2$ , where $X_o$ is the radiation length, which is equal to 37 gm cm$^{-2}$ in air (31).

Thus, the observed electron intensity is given approximately by

$$S(h,E) = \int_E^\infty Z(U,E)G(U,h-\bar{h})dU .$$

A rough estimate was made of the error introduced by neglecting the term in $\frac{\partial^2 G}{\partial h^2}$ . The approximate variation of G with h was obtained from the curves given by Rossi (36) for the intensity of fast mesons and the density of the atmosphere. $\overline{h^2} - (\bar{h})^2$ was obtained for E = 0 from the shower theory under "Approximation B" as given by Rossi and Greisen (34). It was found that, for h = 1000 gm cm$^{-2}$, the error is probably less than 5% and may be much less than that. For extreme accuracy, a more careful estimate of this error should be made.

The three main steps in the evaluation of S(h,E) are the integrations of Equations 5, 6, and 7. The functions which must be known are F(u), the energy distribution of decay electrons, M(h,P), the intensity of mesons, $\varsigma(h)$, the density of the atmosphere, and $\bar{h}(U,E)$. It has been suggested on theoretical grounds by Caianiello (7) that $F(u) = 12u_m^{-4}(u_m-u)\sqrt{u^2-\nu^2}$. This expression is in good agreement with experimental measurements (24, 39). Substituting in Equation 5, we find that $g(U,P) = 6u_m^{-4}\int_{u_1}^{u_2}(u_m-u)udu$ . In evaluating this integral it must be remembered that the integrand is equal to zero for $u > u_m$. $u_2$ is less than $u_m$ only for very small values of U, and numerical calculations for E = 10 Mev indicate that, as mentioned

previously, no appreciable error is introduced by taking the upper limit as $u_m$ rather than $u_2$. The result is that

$$g(U,P) = u_m^{-1}\left[1 - 3(u_1/u_m)^2 - 2(u_1/u_m)^3\right] \quad \text{for } u_1 < u_m$$
$$= 0 \quad \text{for } u_1 > u_m \qquad (9$$

According to Equation 3, $u_1 = U(\sqrt{P^2 - 1} - P)$. Therefore, if $u_1 < u_m$, it follows that $P > P_1 = U/2u_m - u_m/2U$. Thus, $g(U,P) = 0$ for $P < P_1$ and the lower limit in Equation 6 should be taken as $P_1$.

The density, $\rho(h)$, can be obtained from the curve given by Rossi (37). The track length, $Z(U,E)$, has been calculated by Rossi and Klapman (36) for $E = 10$ Mev, and by Richards and Nordheim (31) for large U and various values of E. To correspond to the units used here, the track length must be expressed in gm $cm^{-2}$. The quantity $\bar{h}$ can be obtained from the shower theory under "Approximation B" (34), which is valid for $U \gg \epsilon$, where $\epsilon$ is the critical energy and can be taken as 86 Mev in air (31). It is found that in units of gm $cm^{-2}$, $\bar{h} = 37.4(\log 1.03U - \log 0.69\epsilon)$ for $E = 0$, and $\bar{h} = 37.4\left[\log 1.03U - \log(E + 0.81\epsilon - 0.25\epsilon^2/E)\right]$ for $E > 2\epsilon$. As an interpolation for intermediate values of E, we can use $\bar{h} = 37.4\left[\log 1.03U - \log(E + 0.69\epsilon)\right]$. The quantity $(E + 0.69\epsilon)$ is within 1% of the quantity $(E + 0.89\epsilon - 0.25\epsilon^2/E)$ for all values of E between $2\epsilon$ and $10\epsilon$. The exact form of $\bar{h}$ is not known for small values of U, but another interpolation can be made using the obvious fact that $\lim_{U \to E} \bar{h} = 0$. The resulting expression is

$$\bar{h} = 37.4\left[\log(1.03U - 0.03E + 0.69\epsilon) - \log(E + 0.69\epsilon)\right] \qquad (10$$

This expression is correct for large U and is at least of the right order of magnitude for small U. Numerical calculations

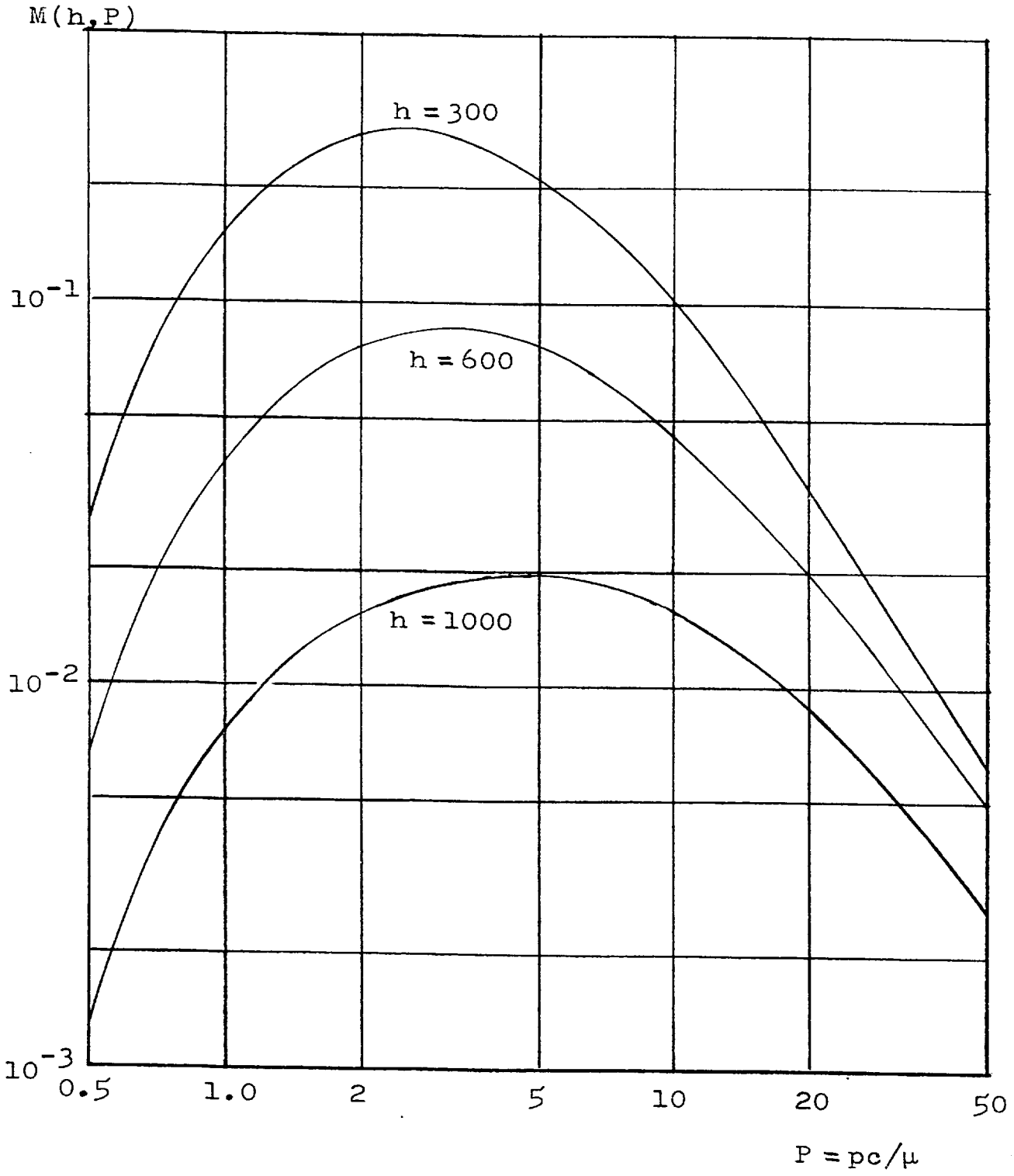
for h = 1000 gm $cm^{-2}$ and E = 10 Mev indicate that 2/3 of the contribution to the final result is from energies U > 500 Mev, which is about 6%. Therefore, the uncertainty in $\bar{h}$ is probably not an important source of error.

The computation, using Equations 6, 8, 9 and 10, was carried out for the vertical direction with h = 1000 gm $cm^{-2}$ and E = 10 Mev. In view of the rather large correction at 10 Mev for scattering in the counter telescope, it might have been better to choose a larger value of E, but the magnitude of this correction was not realized at the time the calculation was made.

The calculations of Rossi and Klapman were used for the track length, Z(U,E) and also for the number of electrons produced by collisions. The greatest uncertainty in the final results is due to insufficient information about the meson spectrum, M(h,P). Many measurements of this quantity have been made at sea level ($\bar{h}$ = 1030 gm $cm^{-2}$), but only a small amount of data is available for higher altitudes. Fig. 7 shows the meson spectrum which was used for P < 50. The curve for h = 1030 is due to Rossi (37) and is based on the results of several different experiments. The curves for h = 300 and h = 600 are taken from the range spectra calculated by Sands (40). The curves of P and dR/dp as functions of R (R = range) given by Rossi (37) were used to convert from a range spectrum to a momentum spectrum. The momentum spectra have been extrapolated in the region below P = 1 by using the experimental data of Nonnemaker and Street (28). The accuracy of this extrapolation is not important since the contribution from

Fig. 8

Differential Meson Spectrum M(h,P)



mesons of $P < 1$ is negligible. Values of $M(h,P)$ for intermediate values of h were obtained by interpolation between the curves of Fig. 7, assuming an exponential variation with h (linear interpolation on a semi-logarithmic plot).

It is likely that Fig. 7 indicates too large a variation with depth for slow mesons ($P < 3$ or 4). Sand's measurements of slow mesons, which were used in calculating the range spectra mentioned above, give a ratio of about 3.3 between Echo Lake and sea level. The measurements made by Kraushaar (23) give a ratio of only 2.4. Fortunately, most of the contribution comes from faster mesons whose variation with depth is less uncertain.

For $P > 50$, it was assumed that $M(h,P)$ is proportional to $P^{-2}$ and varies with h in the same way as at $P = 50$. The measurements of Glaser, Hamermesh, and Sofanov (12) indicate that this is a good approximation at sea level, although at higher altitudes it may be expected that the spectrum falls off more rapidly than at sea level. For very large P the spectrum must fall off more rapidly than $P^{-2}$ because the total momentum of all the mesons must be finite. In order to estimate the error introduced by this assumption, rough calculations were made using $P^{-2}$ with no altitude variation and using $P^{-2.5}$ with the same altitude variation as at $P = 50$. In the former case it was found that the final result (ratio of electrons to mesons) differs by about 5%, and in the latter case by about 0.5%, from the result obtained under the original assumption, which is, therefore considered to be sufficiently accurate.

With the above hypothesis for $M(h,P)$ the integral of Equation 6 can be evaluated analytically in the region above $P = 50$.

For large P, Equation 3 becomes $u_1 = U/2P$, and it follows from Equation 9 that $g(U,P) = 0$ for $P > P_1 = U/2u_m$. Thus, $P_1$ becomes greater than 50 when $U > 100u_m$, and

$$\int_{50}^{\infty} P^{-2} g(U,P) M(h,P) dP = 2500 M(h,50)\, 8u_m^2/15U^3 \qquad \text{for } U > 100u_m$$

$$= 2500 M(h,50) \left[8 \times 10^{-6}/3u_m - 24 \times 10^{-10} U^2/5u_m^3 + 8 \times 10^{-12} U^3/3u_m^4\right] \qquad \text{for } U < 100u_m$$

The integral for $P < 50$ was evaluated graphically for a number of values of U. For each value of U the corresponding value of h, as indicated by Equation 8, is $1000-\bar{h}$, where $\bar{h}$ is obtained from Equation 10. The electron intensity was then computed from Equation 8 by means of another graphical integration. The integrals were evaluated by using a calculating machine to add the ordinates corresponding to small intervals of the abscissa. $\tau$ was taken as 2.15 microseconds. $u_m$ was taken as 53.5 Mev, in agreement with a rest energy of 107 Mev for the meson.

The electron intensity, $S(h,E)$, was found to be 0.106 $cm^{-2}$ $min^{-1}$ $sterad^{-1}$ for h = 1000 gm $cm^{-2}$ and E = 10 Mev. In order to avoid dependence on the normalization of the meson spectrum, which is somewhat in error because of the approximation for $P > 50$, we should consider the ratio of the electron intensity to the meson intensity. The lower limit for penetrating mesons observed in the cloud chamber is P = 150/107 = 1.4 (see Section 3.2). The integral $\int_{1.4}^{\infty} M(1000,P) dP$ was evaluated graphically, giving a meson intensity of 0.577 $cm^{-2}$ $min^{-1}$ $sterad^{-1}$. Comparison with the measurements of Kraushaar (23) indicates that the meson intensity should be about 10% less, but this error is reduced greatly in taking the ratio of electrons to mesons.

Thus the predicted ratio of electrons resulting from decay to mesons is 0.193. Rossi and Klapman (36) give the number of collision electrons with energy greater than 10 Mev as 0.067 of the number of mesons with $P > 2.8$. Corrected to a lower limit of $P = 1.4$, this ratio is 0.064. Consequently the predicted ratio of the number of electrons of energy greater than 10 Mev originating from μ-mesons to the number of μ-mesons with $P > 1.4$ is 0.247.

5.3 Approximate Calculations.

For comparison with the above result, the ratio of decay electrons to mesons was calculated in a simplified way using the method of Rossi, Griesen, and Klapman, which is discussed in Section 5.1. Under the assumption that in the rest system of the meson the electron always receives 1/3 of the energy, it is found that the number of electrons of greater than 10 Mev resulting from the decay of fast mesons is $(0.306\mu/3c\tau)(N/\rho)$, where N is the number of fast mesons and the quantity $N/\rho$ is to be evaluated at a point 3.04 radiation lengths above the point of observation. Taking the radiation length as 37.0 gm $cm^{-2}$ (31), we find that 3.04 radiation lengths is 113 gm $cm^{-2}$. Dividing the above number of electrons by the number of fast mesons at the point of observation gives the ratio of electrons to mesons under the assumption that this ratio is the same when only fast mesons are taken into account as when all mesons are included. Thus, the ratio of electrons to mesons at depth h is given approximately by $(1.69\ 10^{-4}/N_h)(N/\rho)_{h-113}$. Taking N and $\rho$ from the curves given by Rossi (37), we find that at $h = 1000$ gm $cm^{-2}$ the ratio is 0.188. This number is so close to the value 0.183

given in the preceding paragraph that, in view of the uncertainties in the meson spectrum, the lengthy computation used to obtain the latter figure hardly appears justified. It would certainly not be worth while for higher altitudes and larger zenith angles where the meson spectrum is even less well known. Consequently the ratios of electrons from decay to mesons for the other altitudes and zenith angles were calculated only by the simplified method and the resulting figures were multiplied by 0.183/0.188.

There is little experimental evidence concerning the altitude dependence and momentum spectrum of mesons at large zenith angles. Measurements by Jenkins (22) indicate that the zenith angle dependence of fast measons remains the same between sea level and 600 gm $cm^{-2}$, and that at higher altitudes the number of mesons falls off more rapidly with increasing zenith angle. Calculations and measurements by Kraushaar (23) indicate that at sea level the spectrum changes with zenith angle so that there are relatively fewer mesons of low momentum at 60° than at 0°.

As a rough approximation it was assumed that the shape of the meson spectrum is the same at all altitudes and zenith angles and that the variation with zenith angle is the same at all altitudes. Then the ratio of electrons from decay to mesons can be computed for a zenith angle $\theta$ by letting N represent the vertical intensity of fast mesons and evaluating $N/\varrho$ at a point $113\cos\theta$ gm $cm^{-2}$ above the point of observation. It was also assumed that the number of collision electrons is the same everywhere, namely 0.064 times the number of mesons (see Section

5.2). The resulting ratios of numbers of electrons of energy greater than 10 Mev to numbers of penetrating mesons are listed in Table VIII. The figures given for 45° and 60° may involve appreciable errors since the approximations used for the meson intensities have little justification.

TABLE VIII

CALCULATED RATIOS OF ELECTRONS TO MESONS

| | 0° | 45° | 60° |
|---|---|---|---|
| Ann Arbor | 0.247 | 0.229 | 0.220 |
| Echo Lake | 0.346 | 0.312 | 0.293 |
| Mt. Evans | 0.394 | 0.349 | 0.326 |

## 5.4 Correction for Scattering in the Atmosphere.

Probably the largest errors in the ratios of Table VIII, aside from those due to uncertainties in the meson intensities, are caused by use of a one-dimensional model in which the effect of scattering is neglected. No accurate calculations have been made of the angular distribution of low energy electrons in air showers. Roberg and Nordheim (32) have calculated the RMS angular deflections averaged longitudinally over large showers. For large showers the result is independent of the size of the shower. For small showers the scattering should be less, but the angular deflections at production are greater for electrons of low energy. Consequently, the actual RMS deflections, which are averaged over the production spectrum of decay and collision electrons, are probably close to the values calculated by Roberg and Nordheim. By graphical interpolation of their data, it is found that for electrons of energy greater

than 10 Mev the RMS deflection is given by $\alpha = 0.251$ radians or $14.4^\circ$. An approximate correction to the electron intensities can be made by assuming that all electrons are deflected through the angle $\alpha$. Assuming that they are produced with a zenith-angle distribution proportional to $\cos^2\theta$ (a good approximation for electrons produced by mesons, since the angular deviations at production are small), it can be proved (see Appendix II) that the distribution including scattering is proportional to $\cos^2\theta\left[1 - \sin^2\alpha\ (1 - \frac{1}{2}\tan^2\theta)\right]$. Thus, for $\alpha = 14.4^\circ$, the electron intensity at $0^\circ$ should be multiplied by a correction factor $1-\sin^2\alpha = 0.938$, at $45^\circ$ by $1-\frac{1}{2}\sin^2\alpha = 0.969$, and at $60^\circ$ by $1+\frac{1}{2}\sin^2\alpha = 1.031$. Table IX gives the ratios of Table VIII multiplied by these correction factors.

TABLE IX

CORRECTED RATIOS OF ELECTRONS TO MESONS

| | $0^\circ$ | $45^\circ$ | $60^\circ$ |
|---|---|---|---|
| Ann Arbor | 0.232 | 0.222 | 0.227 |
| Echo Lake | 0.324 | 0.302 | 0.302 |
| Mt. Evans | 0.369 | 0.338 | 0.336 |

A rough estimate of the accuracy of this scattering correction was made by assuming that the fractional number of electrons scattered between $\psi$ and $\psi+d\psi$ is equal to $b\ e^{-b\psi}d\psi$. Molière (26) has made an approximate calculation of the distribution function for electrons of all energies, and his function is roughly of this form for angles less than $\pi/4$. Putting $b = 5.6$ gives $\psi_{RMS} = 0.251$, although $b = 7.0$ gives better agreement with Molière's distribution. The correction

to the vertical intensity was calculated with a zenith angle distribution at production of $\cos^2\theta$ for $0 < \pi/2$ and zero for $0 > \pi/2$. It can be demonstrated that the correction factor is given by $b \int_0^{\frac{\pi}{2}} \cos^2\psi \; e^{-b\psi} d\psi$, which, for b greater than about 4, is equal to $1 - 2/(b^2+4)$. Thus, for $b = 5.6$ the correction factor is $1 - 0.057 = 0.943$, in good agreement with the value 0.938 given above. The correction used in undoubtedly less accurate than is indicated by this comparison, but it is probably better than no correction at all.

## Chapter VI

## DISCUSSION OF RESULTS AND CONCLUSIONS

### 6.1 Counting Rates of Penetrating Particles.

The counting rates of penetrating particles were obtained from the data given in Table VI by multiplying the total counting rates by the number of penetrating particles and dividing by the total number of acceptable pictures. These counting rates were divided by $1+C\alpha^2$, using the values of $C\alpha^2$ for $n = 2.1$ from Table VII, in order to correct for the geometry of the counters. The resulting counting rates are listed in Table X. The errors given are the statistical standard deviations, calculated under the assumption that the measurement of the counting rate is independent of the measurement of the number of acceptable pictures. Since these quantities are not completely independent, the true standard deviations are somewhat smaller than those listed. In most cases the uncertainties due to the questionable identification of particles are small compared to the errors listed.

TABLE X

COUNTING RATES OF PENETRATING PARTICLES ($min^{-1}$)

| | 0° | 45° | 60° |
|---|---|---|---|
| Ann Arbor | 0.110 ± .0034 | 0.0454 ± .0015 | 0.0240 ± .0009 |
| Echo Lake | 0.189 ± .0073 | 0.0921 ± .0034 | 0.0402 ± .0019 |
| Mt. Evans | 0.230 ± .0085 | 0.121 ± .0054 | 0.0504 ± .0024 |

Dividing by 0.21 $cm^2$ sterad (see Section 4.4) gives the absolute vertical intensity at Ann Arbor as 0.52 $cm^{-2}$ $sterad^{-1}$ $min^{-1}$ or 0.0087 $cm^{-2}$ $sterad^{-1}$ $sec^{-1}$. Kraushaar (23) has found that at Ithaca (260 meters altitude, compared to 280 meters at

Ann Arbor) the vertical intensity of penetrating particles with minimum range 80 gm $cm^{-2}$ of air (138 gm $cm^{-2}$ of lead) is $0.00887 \pm .00005$ $cm^{-2}$ $sterad^{-1}$ $sec^{-1}$. This figure becomes 0.00904 when corrected to a minimum range of 23 gm $cm^{-2}$ of air (see Section 3.2) by means of Kraushaar's range spectrum. Considering the crudeness of the absolute calibration used for the present experiment, the agreement between 0.0087 and 0.00904 is very satisfactory.

From the data of Table X, the ratio of the vertical intensities at Echo Lake and Ann Arbor is $1.72 \pm .085$. Kraushaar (23) determined that the ratio of the vertical intensities at Echo Lake and Ithaca is $1.71 \pm .02$ for particles capable of penetrating 170 gm $cm^{-2}$ of lead. He found that the ratio for slow mesons is about 2.4 and that at Echo Lake the slow particles include about 20% protons. An approximate correction using these data gives the ratio for particles with minimum range 23 gm $cm^{-2}$ of air as $1.74 \pm .03$, which compares favorably with $1.72 \pm .085$.

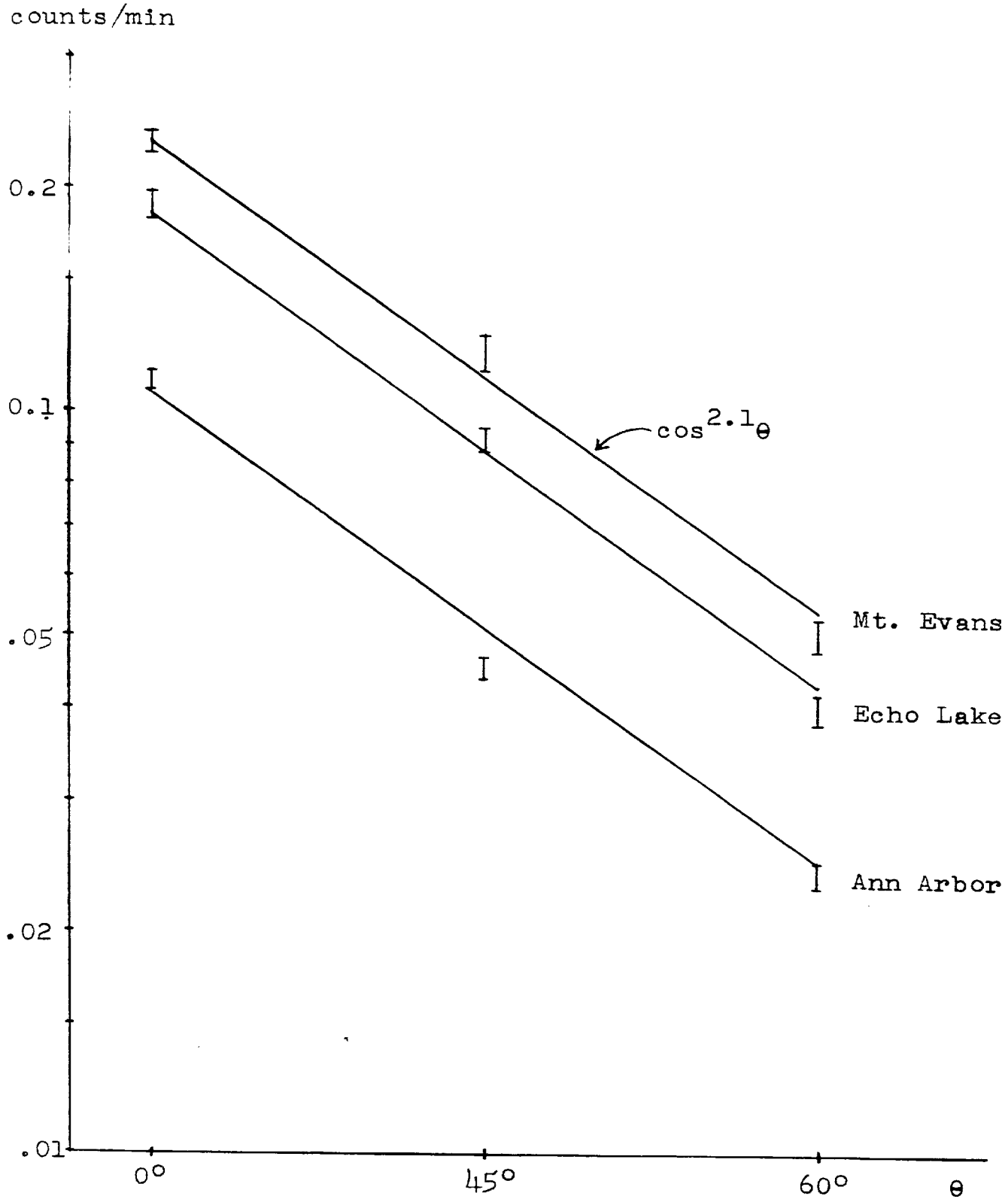
The ratio of the vertical intensities at Mt. Evans and Echo Lake, as determined from Table X, is $1.22 \pm .065$. One of the most careful previous measurements of this quantity is that of Rossi, Hilberry, and Hoag (33), who found counting rates of $11.79 \pm .070$ at Mt. Evans and $9.65 \pm .046$ at Echo Lake, giving a ratio of $1.22 \pm .009$. Their apparatus detected particles capable of penetrating 154 gm $cm^{-2}$ of lead, and the ratio would probably be somewhat higher if corrected to a lower minimum range suitable for comparison with the present experiment.

In Fig. 8 the counting rates of Table X are plotted logrithmically as functions of -log $\cos\theta$, in order to show the dependence on zenith angle. An intensity proportional to $\cos^n\theta$ is represented by a straight line on this graph. The lines shown are drawn with a slope corresponding to $\cos^{2.1}\theta$, in agreement with the results obtained by other investigators. Greisen (14) found $\cos^{2.1}\theta$ for particles penetrating 167 gm $cm^{-2}$ of lead at several altitudes from Ithaca to Mr. Evans. Kraushaar (23) found $\cos^{2.09}\theta$ at Ithaca and $\cos^{2.0}\theta$ at Echo Lake for particles penetrating about the same amount of absorber. He observed that the intensities of slower particles fall off more rapidly with zenith angle, but the correction necessary for comparison with the present data would be very small. The straight lines in Fig. 8 agree with the points as well as might be expected. The point which is farthest off, that at Ann Arbor $45^\circ$, is the one for which the measurement of the counting rate is the most uncertain (see Section 4.1).

Thus the observed counting rates for penetrating particles are in good agreement with the best results obtained by other investigators. Consequently, it appears that if there are any significant systematic errors they must be of such a nature as to affect the numbers of electrons observed without affecting the numbers of penetrating particles.

Fig. 8

Zenith-Angle Dependence of Penetrating Particles



## 6.2 Energy Spectrum of Electrons.

The energy spectra of electrons observed at the various altitudes and zenith angles do not differ by amounts appreciably greater than the statistical errors. This fact is demonstrated by Table XI, which gives the ratios of the number of electrons producing showers of 4 or more track segments to the number penetrating the second plate. The standard deviations for these ratios are all about 0.03.

TABLE XI

RATIO OF NUMBER OF ELECTRONS PRODUCING SHOWERS OF 4 OR MORE TRACK SEGMENTS TO NUMBER PENETRATING THE SECOND PLATE

| Ann Arbor | | | Echo Lake | | | Mt. Evans | | |
|---|---|---|---|---|---|---|---|---|
| 0° | 45° | 60° | 0° | 45° | 60° | 0° | 45° | 60° |
| .26 | .22 | .24 | .24 | .24 | .22 | .24 | .23 | .21 |

Since the various spectra are so nearly the same, they can all be represented approximately by the average spectrum given in Table XII. This spectrum was obtained by adding together all the electrons of each energy range, exclusive of the "Mt. Evans $0^{\circ}_{1}$" column. By combining the data in this way the statistical errors are reduced considerably. Half of the questionable electrons were counted, and the errors listed are the arithmetical sums of the statistical standard deviation and one half the number of questionable electrons. For convenience, the total numbers have been divided by 100.

TABLE XII

INTEGRAL ENERGY SPECTRUM OF ELECTRONS
(not corrected for scattering)

| Min. energy (Mev) | | | 5.1 | 6.9 | 10.4 |
|---|---|---|---|---|---|
| Intensity (arbitrary units) | | | 36.1±1.3 | 33.8±1.2 | 30.0±1.1 |
| 14.4 | 30 | 80 | 125 | 230 | 395 |
| 26.5±1.0 | 17.5±0.8 | 7.06±.43 | 4.77±.31 | 2.62±.21 | 1.23±.13 |

The data of Table XII are plotted in Fig. 9 on a log-log scale. The correction for scattering in the central counter was computed in the way described in Section 4.2 and the corrected spectrum is shown by the solid line extending between 9 Mev and 30 Mev. Above 30 Mev the correction is negligible. Below 9 or 10 Mev the approximations used in calculating the correction become invalid and the error due to scattering in the top wall of the cloud chamber becomes important (see Section 3.1). The corrected intensities for various energies are given in Table XIII, in the same units used in Table XII.

TABLE XIII

INTEGRAL ENERGY SPECTRUM OF ELECTRONS CORRECTED FOR SCATTERING IN THE CENTRAL COUNTERS

| Min. energy (Mev) | 10 | 15 | 20 | 30 |
|---|---|---|---|---|
| Intensity | 34.0 | 27.6 | 23.3 | 17.8 |

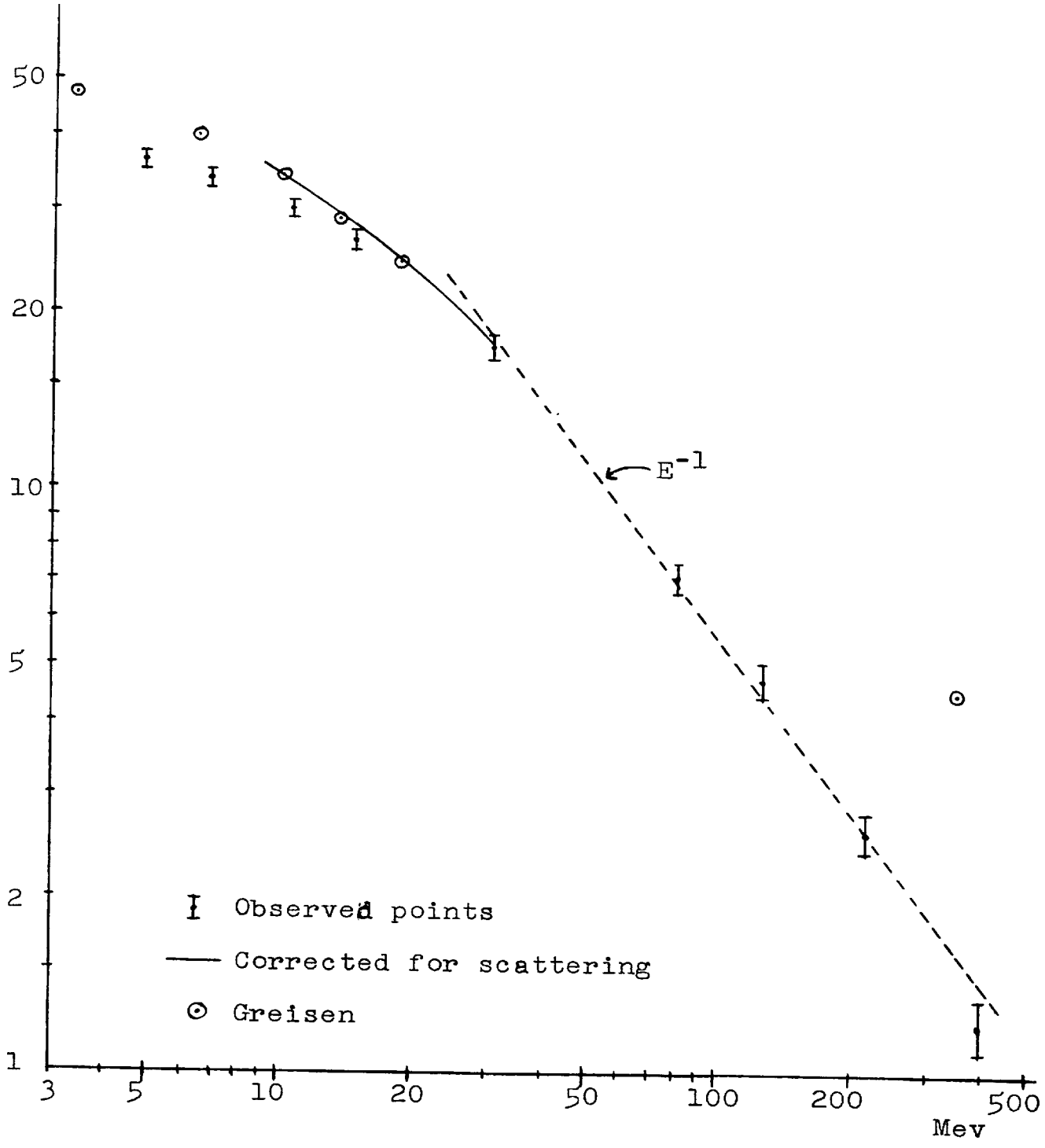
Thus the number of electrons with energy greater than 10 Mev is taken to be 34.0/30.0 times the number observed to penetrate the second plate.

It should be noted that the errors assigned to adjacent points in Fig. 9 are not independent and therefore, if uncer-

Fig. 9

Integral Energy Spectrum of Electrons

(Intensity in arbitrary units)



tainties in the energy are neglected, the shape of the spectrum is determined somewhat better than is indicated by the errors listed. Actually, the errors in energy may be considerably more important than the errors in intensity, but unfortunately they cannot easily be estimated.

As indicated by the dashed line in Fig. 9, the data can be fitted roughly by $E^{-1}$ in the region between 30 and 400 Mev. It appears that at the high energy end the spectrum is falling off more rapidly than $E^{-1}$. This fact is in qualitative agreement with the results obtained by Hazen (17) and extended by Rossi (38) for the spectrum of electrons and photons of very high energy at 10,000 feet altitude.

The points marked with circles in Fig. 9 represent the intensities at low altitude integrated over all directions, as determined by Greisen (15). His figures have been adjusted to agree with the present data at 10 Mev. It will be observed that there is excellent agreement in the shapes of the spectra at the low energy end. The point which Greisen gives at 350 Mev was determined from the electrons penetrating a large thickness of iron. The effects of radiation make it impossible to define a good range-energy relationship for electrons in iron. The value 350 Mev was calculated by means of shower theory but is not to be taken very seriously. Recent calculations, such as those by the Monte Carlo method (48), indicate that the tails of showers extend over considerably greater distances than was previously thought to be the case. Therefore, it is probable that this point actually corresponds to an energy much smaller than 350 Mev. The points at lower energies were determined by

the use of carbon absorbers and should be fairly accurate since the effect of scattering in the apparatus was minimized by counting particles incident from almost all directions.

Comparison of the energy distribution found here with that calculated by Richards and Nordheim (31) for showers with large initiating energies indicates that the calculated distribution is everywhere less steep (decreases more slowly with increasing energy). This result is to be expected because the observed electrons occur in showers which have a continuous range of initiating energies.

A measurement with sufficiently small statistical errors would undoubtedly reveal differences between the energy spectra at different altitudes and zenith angles. In particular, it may be expected that at large zenith angles the number of low energy electrons is relatively larger than near the vertical direction, because of scattering in the air. There is a slight indication of this effect in the ratios of Table XI.

## 6.3 Intensities of Electrons

The ratios of electrons to penetrating particles, derived from Tables V and VI are given in Table XIV for electrons of energies greater than 10, 30, and 80 Mev. The ratios for 10 Mev were obtained by multiplying the number of electrons penetrating the second plate by 34/30, as discussed in the preceding section, and dividing by the number of mesons. The correction factor at 30 Mev is 17.8/17.5. The corrections for the geometry of the telescope (see Section 4.4) are very small and have not been included. The two entries at each position in the table represent the maximum and minimum values obtained by including

or omitting the questionable particles. The errors listed are the statistical standard deviations.

These ratios are in very poor agreement with the results obtained by Greisen (14) in the experiment mentioned in Chapter I. Ratios of electrons to penetrating particles from Greisen's data, n/N in his notation, are listed in Table XV. Here N is the number of particles capable of penetrating 167 gm $cm^{-2}$ of lead, and n is the number of particles which can penetrate 12 gm $cm^{-2}$ of brass plus 1.7 gm $cm^{-2}$ of wood but cannot penetrate the lead. Thus n includes slow mesons and protons as well as electrons. Greisen considers the electrons to have a lower energy limit of about 20 Mev, but the calculations of Section 3.3 indicate that 30 or 40 Mev might be a better guess. The effective energy limit is strongly modified by the effect of scattering in the six thick-walled brass counters and therefore there is little significance in the comparison of the individual values given in Tables XIV and XV. However, the variations with altitude and zenith angle found in the two experiments should be comparable. At $0^{\circ}$ and $45^{\circ}$ the altitude variations agree within the limits of error, but it is evident that the zenith-angle distributions found in the two experiments are inconsistent. Greisen found that the intensities of electrons at all three altitudes could be represented by distributions proportional to $\cos^{3.6}\theta$. It follows that the ratios of electrons to penetrating particles can be represented by $\cos^{1.5}\theta$.

TABLE XIV

OBSERVED RATIOS OF ELECTRONS TO PENETRATING PARTICLES
(Maxima and minima based on uncertainties of identification)

| | | 0° | 45° | 60° |
|---|---|---|---|---|
| Ann Arbor | 10 Mev | $0.298 \atop 0.313 \pm .020$ | $0.256 \atop 0.269 \pm .018$ | $0.291 \atop 0.307 \pm .022$ |
| | 30 Mev | $0.157 \atop 0.165 \pm .013$ | $0.132 \atop 0.140 \pm .011$ | $0.143 \atop 0.154 \pm .014$ |
| | 80 Mev | $0.067 \atop 0.071 \pm .008$ | $0.048 \atop 0.050 \pm .007$ | $0.056 \atop 0.062 \pm .008$ |
| Echo Lake | 10 Mev | $0.806 \atop 0.831 \pm .051$ | $0.511 \atop 0.525 \pm .033$ | $0.473 \atop 0.496 \pm .043$ |
| | 30 Mev | $0.444 \atop 0.462 \pm .029$ | $0.265 \atop 0.274 \pm .021$ | $0.239 \atop 0.250 \pm .022$ |
| | 80 Mev | $0.161 \atop 0.171 \pm .018$ | $0.108 \atop 0.111 \pm .013$ | $0.091 \atop 0.094 \pm .013$ |
| Mt. Evans | 10 Mev | $1.010 \atop 1.045 \pm .052$ | $0.748 \atop 0.814 \pm .050$ | $0.625 \atop 0.641 \pm .043$ |
| | 30 Mev | $0.548 \atop 0.575 \pm .032$ | $0.406 \atop 0.423 \pm .031$ | $0.308 \atop 0.313 \pm .026$ |
| | 80 Mev | $0.213 \atop 0.226 \pm .018$ | $0.161 \atop 0.168 \pm .018$ | $0.113 \atop 0.116 \pm .015$ |

TABLE XV

RATIOS OF ELECTRONS TO PENETRATING PARTICLES FROM GREISEN'S DATA (14)

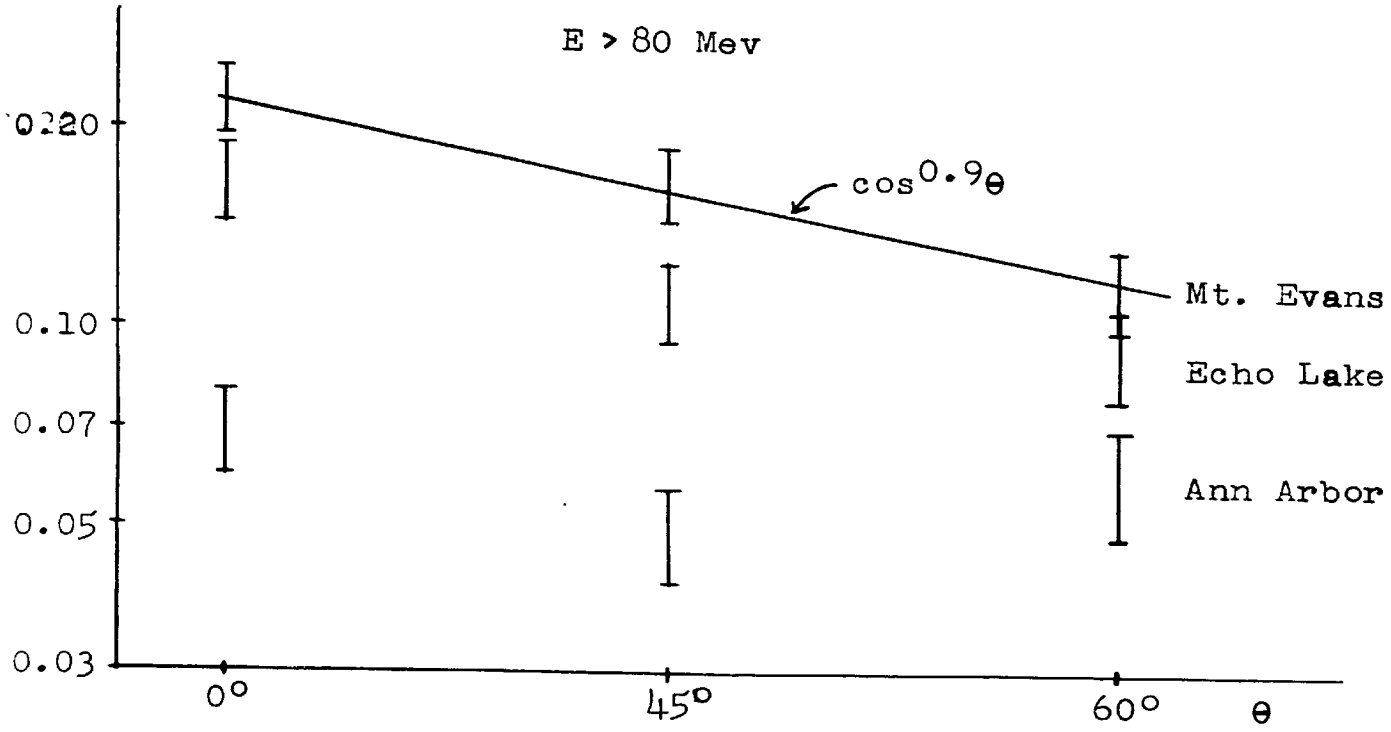
| | 0° | 45° | 60° |
|---|---|---|---|
| Ithaca | 0.26 ± .01 | 0.15 ± .03 | 0.12 ± .03 |
| Echo Lake | 0.58 ± .03 | 0.30 ± .03 | 0.23 ± .04 |
| Mt. Evans | 0.77 ± .02 | 0.49 ± .03 | 0.37 ± .04 |

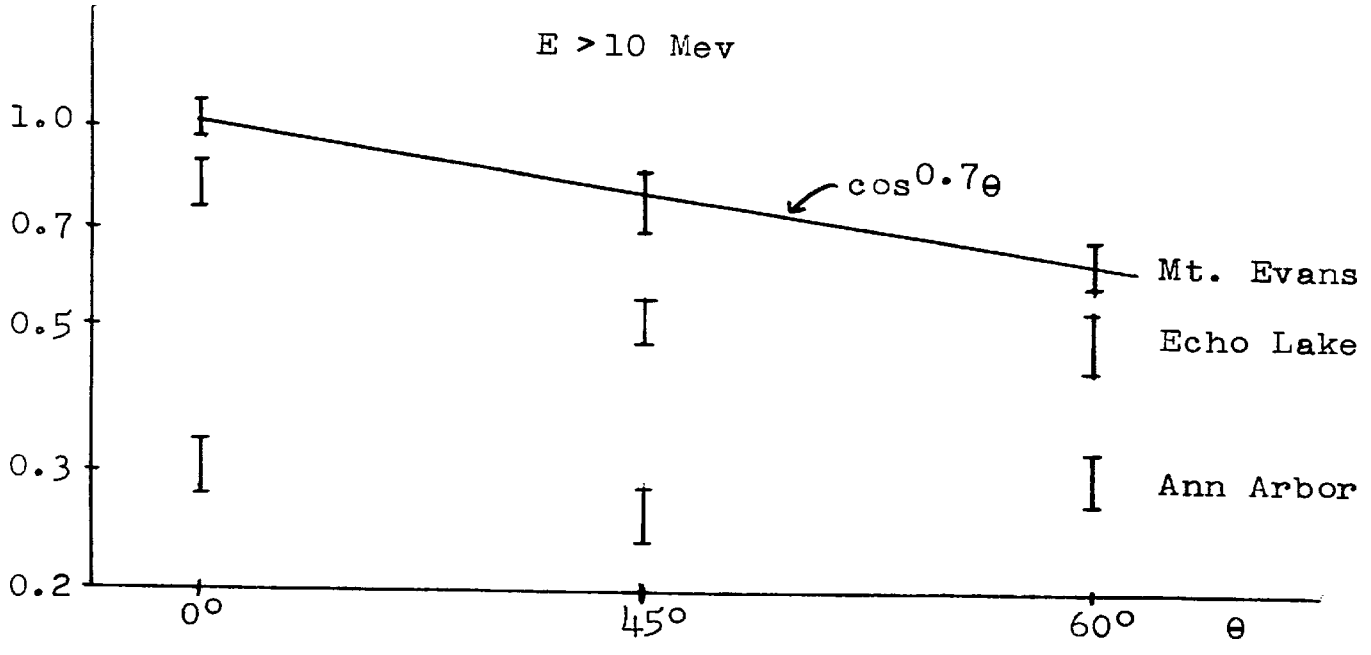
In order to show the zenith-angle dependence of the present data, the ratios for 10 Mev and 80 Mev (from Table XIV) are plotted logrithmically as functions of -log cosθ in Fig. 10. The distribution at Mt. Evans can be represented by $\cos^{0.9}\theta$ for 80 Mev and by $\cos^{0.7}\theta$ for 10 Mev, giving $\cos^{3.0}\theta$ and $\cos^{2.8}\theta$ for the electron intensities. The data for Echo Lake do not fit a $\cos^{n}\theta$ distribution quite as well but the dependence on zenith angle is not very different from that at Mt. Evans. At Ann Arbor, however, the ratios are approximately independent of the zenith angle, as might be expected if most of the electrons originate from mesons.

The fact that the distribution for 80 Mev has the same general form as that for 10 Mev is a good argument against the existence of large errors. The data for the lower energy include all the electrons in the higher range, but these are only about 1/4 of the total number included and therefore the two measurements are almost independent. Thus, if there actually are large errors they must occur in the numbers of electrons of both high and low energies but not in the numbers of penetrating particles. The most likely kind of systematic error depending on the zenith angle is caused by counting particles which did not pass through the counter telescope. However, as mentioned in Section 4.3, errors of this sort should be much larger for electrons of low energy than for those of high energy. Errors due to scattering are also strongly dependent on energy and should be practically independent of zenith angle.

Fig. 10

Ratio of Electrons to Penetrating Particles
as a Function of Zenith Angle



The possibility of large statistical fluctuations cannot be ruled out, but it should be noted that the limits of error indicated in Fig. 10 represent extremely generous estimates. They were obtained by adding the standard deviations listed in Table XIV to the maximum values of the ratios and subtracting them from the minimum values. Since the particles of uncertain identification occur in a similar way at all zenith angles, it is probable that the fraction of them which should be counted is about the same in every case. Therefore it may be assumed that the uncertainties of identification have little influence on the form of the variation with zenith angle.

Inclusion of the electrons occurring multiply would make the zenith-angle distribution slightly steeper. The numbers of these electrons listed in Table VI are upper limits for the numbers that enter the cloud chamber and undoubtedly include many which did not go through the counter telescope. A reasonable guess for the number capable of penetrating the second plate is half the number listed. Including these increases the vertical ratios of Table XIV by 7% at Ann Arbor, 6% at Echo Lake, and 9% at Mt. Evans. The changes at $45^{\circ}$ are much smaller and at $60^{\circ}$ are negligible. These percentages are independent of energy if the energy spectra of multiple electrons and single electrons are the same. The corresponding change in zenith angle distribution is equivalent to an increase of about 0.1 in the exponent of $\cos\theta$.

There cannot be any great error in Greisen's zenith-angle distributions due to the inclusion of slow mesons because, according to Kraushaar (23), the intensities of slow mesons vary

as $\cos^{3.3}\theta$ at Ithaca and as $\cos^{3.1}\theta$ at Echo Lake. The largest errors in Greisen's experiment are certainly those due to scattering, which should be almost independent of the zenith angle. He made no correction for side showers, but their effect should be very small with six-fold coincidences. Thus, it has been impossible to find any satisfactory explanation for the discrepancy between the zenith-angle distributions found in the two experiments.

The unpublished results of an experiment by Palmatier (29) give a zenith angle distribution even steeper than that found by Griesen. In order to minimize the effect of scattering, Palmatier used a triple-coincidence telescope of thin-walled aluminum counters above the absorbers and a large tray of counters below. For electrons capable of penetrating 0.77 gm $cm^{-2}$ of aluminum plus 12.5 gm $cm^{-2}$ of carbon, to which he assigns a lower energy of about 30 Mev, he found distributions proportional to $\cos^{3.8}\theta$ at Ithaca and $\cos^{4.7}\theta$ at Echo Lake. At both altitudes the ratios of electrons to penetrating particles for the vertical direction are consistent with those listed in Table XIV. Palmatier also determined the integral energy spectrum for energies below 30 Mev. His spectrum varies somewhat with altitude and zenith angle but is always less steep than that given in Fig. 10. Part of this discrepancy may be due to differences in the method of determining the energy, but it appears probable that part of it is also due to insufficient corrections for scattering. The relationship between the RMS angle of scattering and the angle defined by the counters in Palmatier's experiment was almost the same as in the present experiment and it does not

appear that adequate corrections were made for scattering in the central counters.

If the intensities of electrons fall off with zenith angle as rapidly as is indicated by the experiments using counters, then it follows that a large proportion of the vertical electrons observed near sea level do not originate from mesons. This conclusion is in disagreement with the value of the vertical intensity derived from the present experiment and with that given by Rossi (37), if the calculations of electrons originating from mesons given in Chapter V are even approximately correct.

In choosing between the results of experiments using counters and of those using cloud chambers, where there are no obvious errors in either, the latter should be considered as more reliable because each event can be considered individually and in greater detail than is possible with counters only. Thus, it appears reasonable to assume that the zenith angle distributions determined here are more nearly correct than those found by means of counters. In order to establish this more certainly, further measurements using cloud chambers should be made.

According to the data of Table XIV, the vertical ratio of electrons of energy greater than 10 Mev to penetrating particles is $0.306 \pm .028$ at Ann Arbor. Taking the vertical intensity of penetrating particles as $0.00904$ cm$^{-2}$ sterad$^{-1}$ sec$^{-1}$ (see Section 6.1), we find that the vertical intensity of the electrons is $0.00276 \pm .00025$ cm$^{-2}$ sterad$^{-1}$ sec$^{-1}$. The curve deduced by Rossi for the vertical intensities of electrons capable of penetrating 5 gm cm$^{-2}$ of brass gives $0.0022$ cm$^{-2}$ sterad$^{-1}$ sec$^{-1}$

for the altitude of Ann Arbor. Rossi assigns a lower energy limit of 10 Mev to these electrons, but it is probable that, due to scattering, not all electrons above this energy were included. Therefore a somewhat higher equivalent energy limit should be used for comparison with the present data. According to the energy spectrum of Fig. 9, a limit of 15 Mev would bring Rossi's vertical intensity into agreement with the value found above. However, for the altitude of Mt. Evans, Rossi's curve gives an intensity of 0.021 $cm^{-2}$ $sterad^{-1}$ $sec^{-1}$, while the data of Table XIV and Section 6.1 give 0.0194 .0013 $cm^{-2}$ $sterad^{-1}$ $sec^{-1}$. Thus it is apparent that Rossi's curve gives a more rapid rate of increase with altitude than is found in the present experiment, and that near sea level the absolute values of the intensities are in fairly good agreement.

The integrated intensity, J, is defined by $J = 2\pi \int_0^{\frac{\pi}{2}} I \sin\theta \, d\theta$, where I is the directional intensity and $\theta$ is the zenith angle. If $I = I_o \cos^n\theta$, then $J = 2\pi I_o/(n-1)$. Thus if n = 2.1 for electrons with energy greater than 10 Mev, as is indicated by Fig. 10, the integrated intensity of these electrons at Ann Arbor is given by $2\pi(0.00276 \pm .00025)/3.1 = 0.0056 \pm .0005$ $cm^{-2}$ $sec^{-1}$. Kraushaar (23) has deduced a value of 0.0060 $cm^{-2}$ $sec^{-1}$ for the same quantity at Ithaca, using the results of a measurement by Greisen (43). The agreement is very satisfactory, although not particularly significant in view of the uncertainty in n.

## 6.4 Electrons Originating From Nuclear Interactions.

As mentioned in Chapter I, the excess electrons which do not originate from $\mu$-mesons are presumed to originate from nuclear

interactions. A few electrons are produced by collision processes of protons, but their effect is negligible since, due to the large mass of the proton, the maximum transferable energy is small.

The numbers of excess electrons may be obtained from the difference between the observed numbers of electrons and the calculated numbers of electrons originating from mesons. The former are given in Table XIV as ratios of electrons to penetrating particles. The latter are given in Table IX as ratios of electrons to mesons. These should be corrected to include the protons in the penetrating particles, but that is difficult because the intensities of protons at large zenith angles are not known. If it is assumed that the vertical intensities of penetrating particles include 6% protons at Mt. Evans, 4% at Echo Lake, and 0.75% at Ann Arbor (Section 3.2), then the vertical intensities of the excess electrons are increased by about 3% at each altitude and the form of dependence on altitude (see below) is not changed. In taking the observed numbers of electrons from Table XIV, the averages of the maximum and minimum values were used and the errors were taken as the statistical standard deviations plus half the difference between the maximum and minimum ratios.

The differences obtained without correcting for protons were multiplied by 1.72 for Echo Lake and $1.72 \times 1.22 = 2.10$ for Mt. Evans (Sec. 6.1) in order to show the dependence of the excess electrons on altitude. Also, to make the dependence on zenith angle more apparent, the figures for $45^\circ$ were multiplied by $\cos^{2.1} 45^\circ = 0.485$ and those for $60^\circ$ by $\cos^{2.1} 60^\circ = 0.234$. The

numbers obtained in this way are listed in Table XVI and represent the intensities of the excess electrons divided by the vertical intensity of penetrating particles at Ann Arbor, which, as we have seen, is 0.0090 $cm^{-2}$ $sterad^{-1}$ $sec^{-1}$. In order to take into account the protons in the penetrating component, it may be considered that these numbers represent the intensities of excess electrons in units of 0.0087 $cm^{-2}$ $sterad^{-1}$ $sec^{-1}$ (see preceding paragraph).

TABLE XVI

INTENSITIES OF EXCESS ELECTRONS WITH ENERGY >10 MEV

In units of: 0.0087 $cm^{-2}$ $sterad^{-1}$ $sec^{-1}$

| | 0° | 45° | 60° |
|---|---|---|---|
| Ann Arbor | 0.074 ± .028 | 0.019 ± .012 | 0.017 ± .007 |
| Echo Lake | 0.85 ± .11 | 0.179 ± .033 | 0.071 ± .022 |
| Mt. Evans | 1.38 ± .15 | 0.450 ± .084 | 0.147 ± .025 |

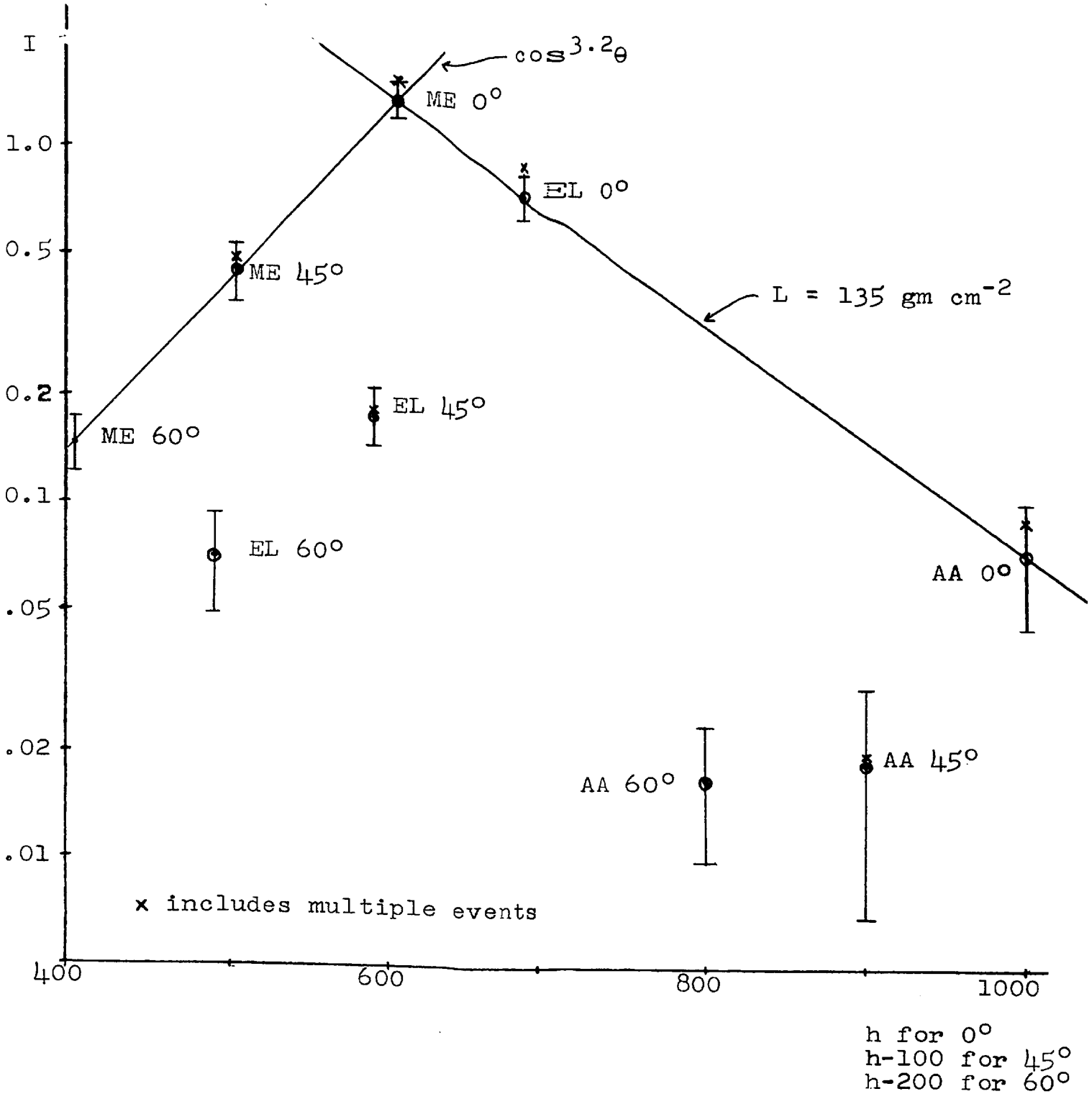
At 0° the errors listed probably represent a good estimate of the actual uncertainties. At 45° and 60°, however, the uncertainties in calculated numbers of electrons from mesons are large. At Ann Arbor the percentage errors are increased greatly because the intensities listed come from the differences between two almost equal quantities. The situation becomes better at higher altitudes where the calculated intensities are smaller fractions of the observed intensities. Thus, very little reliance can be placed in the intensities of excess electrons for 45° and 60° at Ann Arbor, but the values for 45° and 60° at Echo Lake and Mt. Evans can be considered as fairly good.

In Fig. 11, the intensities from Table XVI are plotted logarithmically against the atmospheric depth h. The points

Fig. 11

Intensities of Electrons from Nuclear Interactions

(In units of 0.0087 $cm^{-2} sterad^{-1} sec^{-1}$)



for 45° are offset by 100 gm $cm^{-2}$ to the left of those for 0°, and the points for 60° are offset by another 100 gm $cm^{-2}$. Thus, for a given altitude the graph may be considered as a plot of intensity against log cosθ and a zenith-angle dependence of $\cos^n\theta$ will be represented by a straight line.

The variation of the vertical intensity with atmospheric depth is represented very well by an expression of the form $e^{-h/L}$, with L = 135 gm $cm^{-2}$, as can be seen from the straight line drawn through the 0° points. A rough estimate of the uncertainty in L, based on the errors given for the points, is 15 gm $cm^{-2}$. The zenith angle dependence at Mt. Evans is well represented by $\cos^{3.2}\theta$.

The points marked with x's represent the intensities obtained when the electrons occurring multiply are included in the observed intensities. As in Section 6.3, the numbers of multiple electrons were taken as half numbers listed in Table VI. Inclusion of these electrons does not appreciably affect the altitude dependence of the vertical intensity, but does make the zenith angle variation somewhat steeper so that at Mt. Evans the exponent of cosθ is increased from 3.2 to 3.4.

Due to the uncertainties mentioned above, the altitude dependence at 45° and 60° cannot be determined very accurately from the present data. It appears from Fig. 11 that this dependence is approximately the same as that at 0°. It follows that the zenith angle dependence at Echo Lake and Ann Arbor is approximately the same as at Mt. Evans.

The observed altitude dependence, with an absorption thickness of L = 135 gm $cm^{-2}$ is in good agreement with the

hypothesis that the excess electrons originate from nuclear interactions. As previously mentioned, Mylroi and Wilson (27) give $L = 143 \pm 13$ for the altitude variation of the vertical intensity of protons. Observations of events associated with nuclear interactions give a steeper dependence on altitude. Tinlot (46) measured the altitude dependence of penetrating showers (interactions in which two or more penetrating particles are produced) and found an absorption length of $118 \pm 2$ gm $cm^{-2}$. Bridge and Rossi (5) studied bursts in an ionization chamber at various depths and concluded that the radiation responsible for nuclear interactions has an absorption length of 107 gm $cm^{-2}$. It is likely that the lower energy limit of events detected by their apparatus was considerably higher than in the case of Tinlot's experiment, and therefore Tinlot's results are probably more suitable for comparison with the data on excess electrons.

There is very little evidence available concerning the zenith angle dependence of particles associated with nuclear interactions. Miller, et al. (25a) found that at an altitude of 3300 meters the intensity of protons with momentum less than 1 Bev/c decreases by a factor of 3 from $0^\circ$ to $45^\circ$. If a variation of the form $\cos^n\theta$ is assumed, the resulting exponent is 3.2, in excellent agreement with the value found above for excess electrons.

As a simple assumption, an expression of the form $e^{-h/L\cos\theta}$ might be considered suitable to represent the dependence on atmospheric depth and zenith angle of the events associated with nuclear interactions. This expression results from the assump-

tions that the primary particles are isotropic above the atmosphere, that the primaries and any interacting secondaries have an absorption length L in the atmosphere, that the effects of competition between nuclear interactions and decay of secondaries such as π-mesons is negligible, and that the original direction of a primary is preserved by all of its secondaries. The assumption of isotropy is reasonable because only primaries of very high energy, which are not affected greatly by the earth's magnetic field, can contribute appreciably to the interactions observed at large atmospheric depths. The existence of interacting secondaries with absorption lengths different from that of the primaries would not have much effect on the general form of the distribution. The effect of the competition between interaction and decay is to make the intensity fall off more rapidly with zenith angle, because particles at large zenith angles spend a long time in the upper part of the atmosphere where the density is low and the probability of decay is large compared to the probability of interaction. On the other hand, the effect of deviations between the directions of primaries and secondaries is to make the intensity fall off less rapidly with zenith angle.

An expression of the above form is in complete disagreement both with the previously mentioned measurements of low energy protons and with the present measurements of electrons associated with nuclear interactions. With any reasonable value for L, such an expression gives a decrease of intensity with zenith angle which is many times the observed decrease. It also gives a dependence on altitude which is much steeper

at large zenith angles than in the vertical direction, in apparent contradiction to the data of Fig. 11. In the case of low energy protons it may be expected that the assumption of the preservation of direction is not valid and that the zenith-angle distribution should not agree with the above expression. In the case of the electrons we may conclude that the assumption of the preservation of direction is also invalid.

As we have seen in Section 5.3, the RMS angular spread of showers is about 15° for electrons of energy greater than 10 Mev, and the resulting effect on the zenith-angle distribution is rather small. For steeper initial distributions the effect is larger, but it certainly is not sufficient to explain the observed results. Thus, there must be large angular deviations in the production and decay processes of the neutral π-mesons from which the electrons are believed to originate. We can conclude, therefore, that the average energy of the neutral π-mesons is not large compared to the rest energy.

## 6.5 Summary of Results and Conclusions.

A. Penetrating Particles. We have found that the zenith angle dependence of penetrating particles (range 23 gm $cm^{-2}$ of air equivalent) at Ann Arbor, Echo Lake, and Mt. Evans can be represented by $\cos^{2.1}\theta$. The measured ratio of the vertical intensities at Echo Lake and Ann Arbor is $1.72 \pm .085$, and the corresponding ratio for Mt. Evans and Echo Lake is $1.22 \pm .065$. These results are in excellent agreement with those obtained by other investigators.

B. Energy Spectrum of Electrons. Within the statistical errors, the observed energy spectra are the same for the vario

altitudes and zenith angles. An average energy spectrum, corrected for scattering in the counter telescope, is given in Fig. 9. The shape of this spectrum, in the region of low energies, is in good agreement with that determined by Greisen (15) in measurements of the integrated intensity near sea level.

C. Intensities of Electrons. The observed intensities of electrons, in terms of the intensities of penetrating particles, are given in Table XIV and Fig. 10. The decrease of intensity with zenith angle is found to be much less than has been reported by other investigators. The ratio of electrons to penetrating particles is approximately independent of zenith angle at Ann Arbor. The verticle intensity of electrons of energy greater than 10 Mev is $0.00275 \pm .00025$ $cm^{-2}$ $sterad^{-1}$ $sec^{-1}$ at Ann Arbor, in fairly good agreement with the results of other experiments. The vertical intensity increases with altitude somewhat more slowly than has been indicated by Rossi (37).

D. Electrons Originating From Mesons. The number of electrons originating from μ-mesons has been calculated by a lengthy and fairly complete method for the vertical direction at Ann Arbor. An approximate calculation has been made for other directions and altitudes and an attempt has been made to include the effects of scattering in the atmosphere (Table IX). The accuracy of these calculations is limited by the lack of knowledge of the momentum spectrum of mesons as a function of altitude and zenith angle.

E. Electrons Originating From Nuclear Interactions. The difference between the number of electrons observed and the number calculated to originate from μ-mesons is assumed to represent the number originating from nuclear interactions. This assumption is supported by the altitude dependence of the vertical intensities, which is found to be exponential with an absorption length of $135 \pm 15$ gm $cm^{-2}$. The dependence on zenith angle is represented approximately by $\cos^{3.2}\theta$ at Mt. Evans, and is much less steep than would be expected if the electrons preserved the directions of the primary particles from which they originated. The difference is greater than can be explained by the scattering of the electrons, and therefore it is concluded that the average energy of the neutral π-mesons from which the electrons originate must be relatively small.

# APPENDIX I

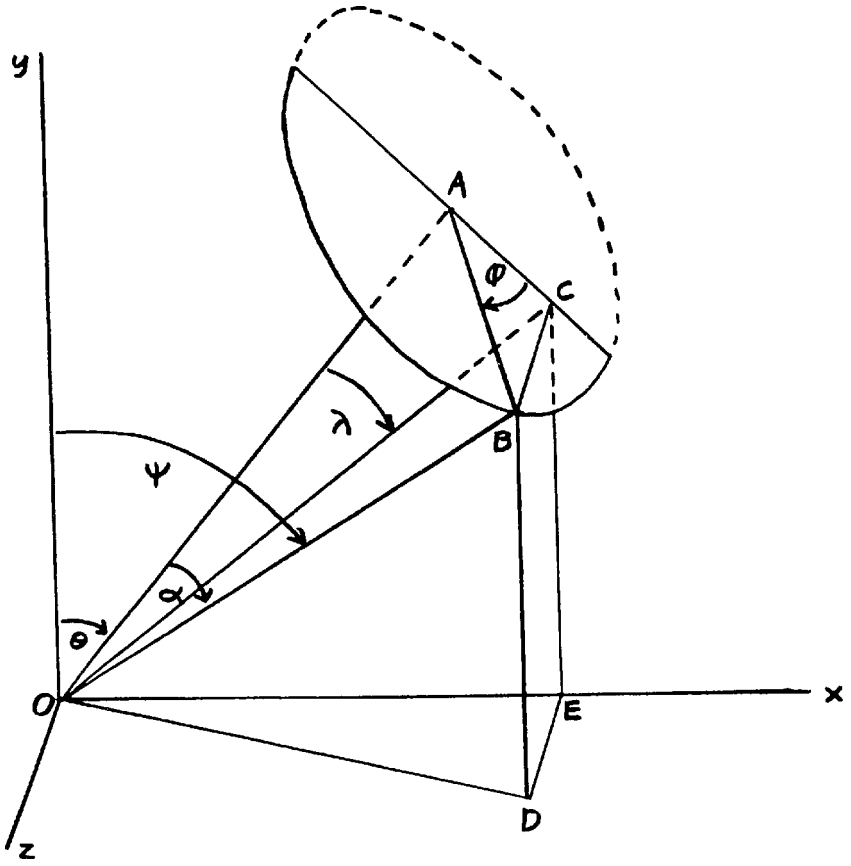
## DEFINITIONS OF SYMBOLS

| | |
|---|---|
| A | Atomic weight |
| $\beta$ | Velocity divided by c |
| c | Velocity of light ($3.00 \times 10^{13}$ cm/sec) |
| E | Total energy |
| $\mu$ | Rest energy of heavy particle (107 Mev for $\mu$-meson) |
| $\nu$ | Rest energy of electron (0.511 Mev) |
| $N_o$ | Avogadro's number ($6.02 \times 10^{23}$) |
| p | Momentum |
| P | "Reduced momentum" ($pc/\mu$) |
| $\rho$ | Density on gm $cm^{-2}$ |
| $r_o$ | Classical radius of the electron ($e^2/mc^2 = 2.818 \times 10^{-13}$ cm) |
| u | Total energy of decay electron in rest system of meson |
| $u_m$ | Maximum value of u (53.5 Mev) |
| U | Total energy of decay electron in laboratory system |
| Z | Atomic number |

## APPENDIX II

## EFFECT OF SCATTERING ON ANGULAR DISTRIBUTION

Assume that a group of particles are produced with a zenith-angle distribution of $\cos^2\psi$, and are all scattered by an angle $\alpha$ from their original directions.




A particle which is observed along the direction OA, at zenith angle $\theta$, must have been produced in some direction, OB, lying in the circular cone with axis OA and half angle $\alpha$. Let the zenith angle of OB be $\psi$. Let OA lie in the xy plane and $\phi$ be the angle between the xy plane and the plane OAB. The intensity observed along OA can be found by averaging $\cos^2\psi$ over all possible positions of OB. Due to symmetry, it is sufficient

to let $\phi$ vary from 0 to $\pi$. Thus, the directional intensity at zenith angle $\theta$ is proportional to $I(\theta) = \frac{1}{\pi}\int_0^{\pi}\cos^2\psi\, d\phi$. To find $\cos^2\psi$ in terms of $\phi$, let OC be the projection of OB on the xy plane and OD the projection of OB on the xz plane. Then $\cos\psi = BD/OB$, $BD = CE = OC\cos(\theta+\lambda)$, $OB = OA/\cos\alpha$, and $OC = OA/\cos\lambda$. It follows that $\cos\psi = \frac{\cos\alpha\,\cos(\theta-\lambda)}{\cos\lambda}$. Making use of the fact that $\tan\lambda = \tan\alpha\cos\phi$, we find that $\cos^2\psi = \cos^2\alpha\,(\cos^2\theta - 2\sin\theta\cos\theta\tan\alpha\cos\phi + \sin^2\theta\tan^2\alpha\cos^2\phi)$. Evaluation of the integral gives $I(\theta) = \cos^2\alpha\cos^2\theta + \frac{1}{2}\sin^2\alpha\sin^2\theta$, which can be reduced to $I(\theta) = \cos^2\theta\left[1 - \sin^2\alpha\,(1 - \frac{1}{2}\tan^2\theta)\right]$.

BIBLIOGRAPHY


1 P. R. Barker, Phys. Rev. 81, 291 (51)

2 I. B. Bernstein, Phys. Rev. 80, 995 (50)

3 F. A. Berry, E. Bollay, N. R. Beers, Handbook of Meteorology, McGraw-Hill, New York 1945

4 R. Bjorklund, W. E. Crandall, B. J. Moyer, H. F. York, Phys. Rev. 77, 213 (50)

5 H. S. Bridge, B. Rossi, Phys. Rev. 75, 810 (49)

6 W. W. Brown, A. S. McKay, E. D. Palmatier, Phys. Rev. 76, 506 (49)

7 E. R. Caianiello, Nuovo Cimento 7, 749 (51)

8 C. Y. Chao, Phys. Rev. 75, 581 (49)

9 C. L. Critchfield, E. P. Ney, S. Oleska, Phys. Rev. 79, 402 (50)

10 W. A. Fowler, C. C. Lauritson, T. Lauritson, Rev. Mod. Phys. 20, 236 (48)

11 W. M. Fretter, Phys. Rev. 73, 41 (48) and 76, 511 (49)

12 D. A. Glaser, B. Hamermesh, G. Sofanov, Phys. Rev., 80, 625 (50)

13 B. P. Gregory, B. Rossi, J. H. Tinlot, Phys. Rev. 77, 299 (50)

14 K. I. Greisen, Phys. Rev. 61, 212 (42)

15 K. I. Greisen, Phys. Rev. 63, 323 (43)

16 E. P. Gross, Range, Ionization Curves, Princetcn Univ. 1947

17 W. E. Hazen, Phys. Rev. 65, 67 (44)

18 W. Heitler, The Quantum Theory of Radiation, Oxford University Press 1947

19 F. L. Hereford, C. P. Swann, Phys. Rev. 78, 727 (50)

20 R. B. Hulsizer & B. Rossi, Phys. Rev. 73, 1402 (48)

21 International Critical Tables, Vol. 2, pp 93, 110 McGraw-Hill, New York 1927

22 J. F. Jenkins, Jr., Phys. Rev. 76, 992 (49)

23 W. L. Kraushaar, Phys. Rev. 76, 1045 (49)

24 R. B. Leighton, C. D. Anderson, A. J. Seriff, Phys. Rev., 75, 1432 (49) and 76, 159 (49)

25 Mathematical Tables Vol. 1, Brit. Assoc. Adv. Sci. London 1931

25a C. E. Miller, J. E. Henderson, G. Garrison, W. Sandstrom, Phys. Rev. 85, 723 (52)

26 G. Moliere, Cosmic Radiation. W. Heisenberg, Ed., Dover Publications, New York 1946

27 M. C. Mylroi & J. G. Wilson, Proc. Phys. Soc. A, 64, 404 (51)

28 G. M. Nonnemaker & J. C. Street, Phys. Rev. 82, 564 (51)

29 E. D. Palmatier, Thesis, Cornell University 1951

30 G. J. Perlow & C. W. Kissinger, Phys. Rev. 81, 552 (51)

31 J. A. Richards & L. W. Nordheim, Phys. Rev. 74, 1106 (48)

32 J. Roberg & L. W. Nordheim, Phys. Rev. 75, 444 (49)

33 B. Rossi, N. Hilberry, J. B. Hoag, Phys. Rev. 57, 461 (40)

34 B. Rossi & K. Greisen, Rev. Mod. Phys. 13, 240 (41)

35 B. Rossi & K. Greisen, Phys. Rev. 61, 121 (42)

36 B. Rossi & S. J. Klapman, Phys. Rev. 61, 414 (42)

37 B. Rossi, Rev. Mod. Phys. 20, 537 (48)

38 B. Rossi, Rev. Mod. Phys. 21, 104 (49)

39 R. Sagane, W. L. Gardner, H. W. Hubbard, Phys. Rev. 82, 557 (51)

40 M. Sands, Phys. Rev. 77, 180 (50)

41 M. Schein, W. P. Jesse, E. O. Wollan, Phys. Rev. 57, 615 (41)

42 A. M. Shapiro, Phys. Rev. 82, 307 (51)

43 A. M. Shapiro, Private Communication, 1951

44 H. S. Snyder, Phys. Rev. 76, 1563 (49)

45 J. Steinberger, W.K.H. Panofsky, J. Steller, Phys. Rev. 78, 802 (50)

46 J. Tinlot, Phys. Rev. 74, 1197 (48)

47 R. R. Wilson, Phys. Rev. 60, 749 (41)

48 R. R. Wilson, Phys. Rev. 86, 261 (52)

49 J. A. Wheeler & W. E. Lamb, Phys. Rev. 55, 858 (39)

